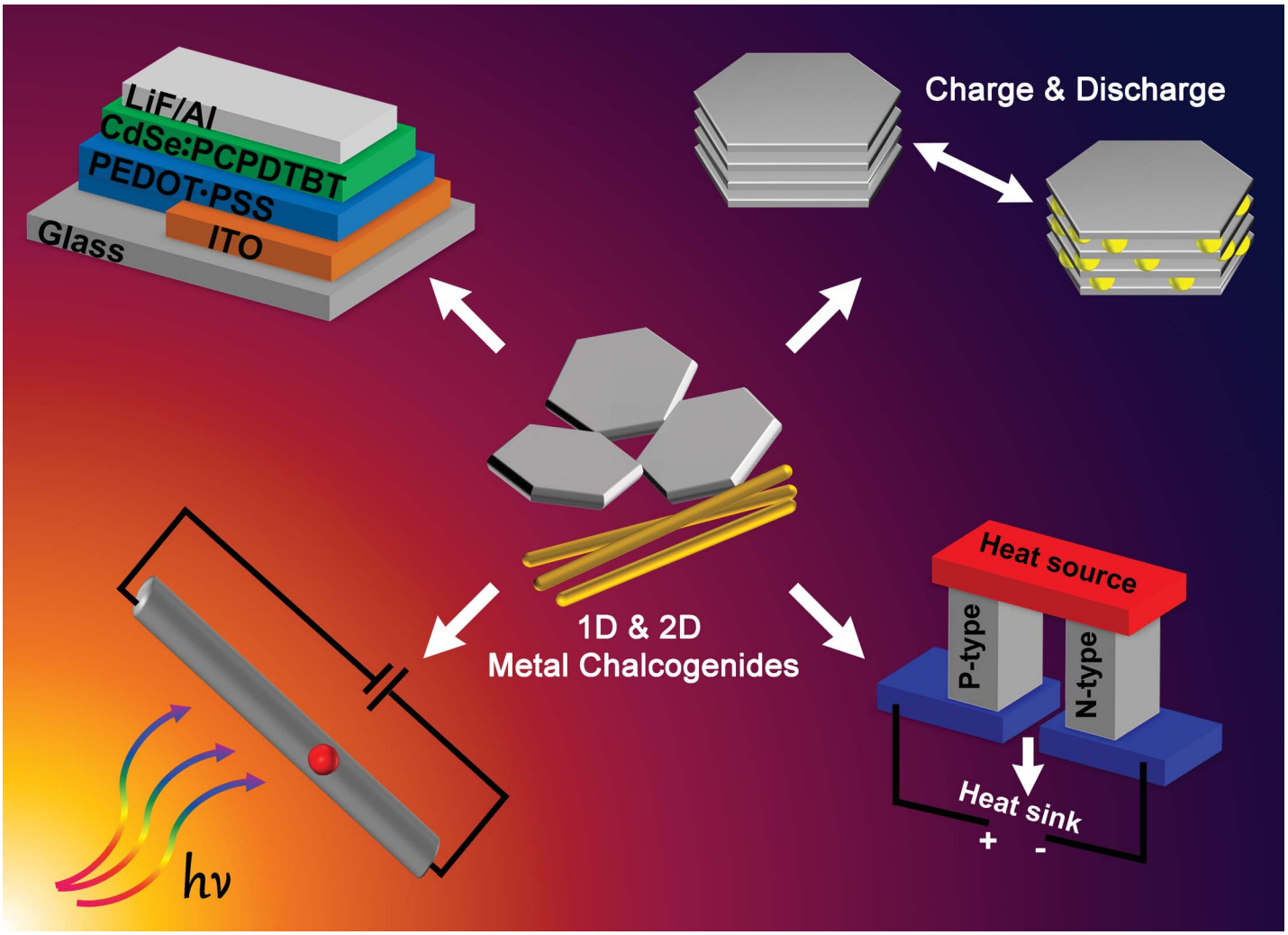

A feature article from the Hybrid Nano Materials Laboratory of Prof. Unyong Jeong (Yonsei Univ., Korea) with collaboration from the Materials Theory Group of Prof. Aloysius Soon (Yonsei Univ., Korea).

Title: Solution-based synthesis of anisotropic metal chalcogenide nanocrystals and their applications

Anisotropic metal chalcogenide nanocrystals have been intensively investigated in recent years because of their high potential for use in a wide variety of applications. Recent advances in solution-based synthesis and the practical applications of these nanomaterials are reviewed and practical challenges are discussed in this article.

As featured in:

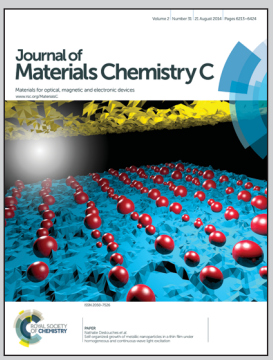

See Unyong Jeong *et al.*, *J. Mater. Chem. C*, 2014, **2**, 6222.

ROYAL SOCIETY OF CHEMISTRY

www.rsc.org/MaterialsC

Registered charity number: 207890

Journal of Materials Chemistry C

FEATURE ARTICLE

View Article Online
View Journal | View Issue

Cite this: J. Mater. Chem. C, 2014, 2, 6222

Solution-based synthesis of anisotropic metal chalcogenide nanocrystals and their applications

Yuho Min,† Geon Dae Moon,† Chang-Eun Kim, Ji-Hwan Lee, Heesung Yang, Aloysius Soon and Unyong Jeong*

This article reviews recent advances in solution phase synthesis to generate 1-D and 2-D anisotropic metal chalcogenide (MC) nanostructures with a focus on using different growth mechanisms to control the shapes of the MCs. Four different synthetic approaches have been reviewed: naturally favoured growth due to its intrinsically anisotropic crystal structure, modified anisotropic growth by changing surface energies or utilizing organic templates, oriented attachment of small nanocrystal building blocks to form nanowires or nanosheets, and chemical transformation from existing nanostructures into new species. We discuss current understanding of the thermodynamic and kinetic aspects associated with the mechanisms of forming these anisotropic MC nanostructures. We provide examples of representative applications of anisotropic chalcogenide nanomaterials that are expected to be practically meaningful in the near future. The applications include electrodes for lithium ion batteries, photodetectors, thermoelectric devices, and solar cells. A brief review of other potential applications (oxygen reduction reaction, localized surface plasmon resonance, topological insulator, superconductor) is provided as well. This review ends with discussions on the challenges to be investigated thoroughly in the solution-based synthesis of anisotropic nanomaterials, which includes surface energy control, correcting the nucleation & growth mechanism, removal of the organic surfactant, kinetic study on the chemical transformation, scale-up of production, and eco-friendly synthesis.

Received 24th March 2014
Accepted 15th May 2014

DOI: 10.1039/c4tc00586d

www.rsc.org/MaterialsC

1. Introduction

Having the ability to exert control over the shape of nanocrystals has always been desired and essential to tune their chemical or physical properties for target applications.[1–3] Anisotropic

Department of Materials Science and Engineering, Yonsei University, 134 Shinchon-dong, Seoul, Korea. E-mail: ujeong@yonsei.ac.kr

† The authors equally contributed to this work.

Yuho Min received a B.S. degree in the Dept. of Materials Science and Engineering from Yonsei University in 2010. He is pursuing his Ph.D. degree under the supervision of Prof. Unyong Jeong in the same department. His research interests include synthesis of metal chalcogenide nanomaterials and solid-state device materialization of inorganic nanocrystals for their opto-electronic and thermoelectric applications.

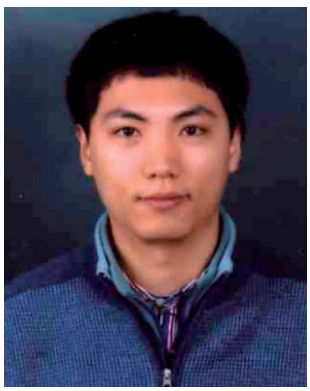

Geon Dae Moon received a B.S. in 2006 and Ph. D. in 2011 in the Dept. of Materials Science and Engineering from Yonsei University under the supervision of Prof. Unyong Jeong. Then, he worked as a postdoctoral fellow in Prof. Yadong Yin's group in the Dept. of Chemistry in University of California, Riverside. Now, he has been working as a research associate in the Sustainable Energy Technology Dept., Brookhaven National Laboratory since 2013. His research interests include synthesis of metal, metal oxide, and metal chalcogenide nanomaterials along with self-assembly of those inorganic nanostructures for electronic and electrochemical applications.

nanocrystals have unique properties that are direction-dependent and have the ability to confine the motion of electrons, holes, excitons, phonons, and plasmons in specific and controlled directions.[1,3] Such uniqueness has been employed in electronics (conducting platforms, transistors, electromechanical devices),[4–7] energy conversion and storage devices (Li ion batteries, solar cells, thermoelectrics, piezoelectrics),[8–17] optical devices (lasers, OLEDs, photodetectors),[18–21] and electrochemical devices (catalysis, gas sensors).[22,23] Anisotropic nanocrystals have been observed in many materials including carbons, silicon, metals, metal oxides, chalcogenides, carbides, nitrides, and their compounds.[24,25]

Although anisotropic metal chalcogenide (MC) nanocrystals have recently been investigated with much interest (with regard to their applications), remarkable advances have been made with anisotropic nanocrystals in diverse areas of modern technology.[1] These MC nanocrystals are also strong candidate materials for thermoelectric devices. Energy harvested from heat loss and cooling electronic devices by effective heat transfer has motivated the studies on the chalcogenide-based thermoelectric devices.[26] In photovoltaic and photodector devices, MC nanocrystals have shown to absorb sun light; hence they can function as exiton generators and charge transport materials.[27–29] The MC nanocrystals with a layered crystal structure and their composites with carbon materials are promising candidates that can intercalate Li^+ ions reversibly, which can be used as electrodes for batteries.[30–33] In addition to these applications, novel applications are recently being investigated for these MCs. As an alternative to noble metals, doped MC nanostructure has attracted interest as an efficient catalyst for the oxygen reduction reaction[34,35] and as a patternable material whose localized surface plasmon resonance is tunable.[36,37] The topological insulating characteristics[38] and superconductivity[39] of MC nanostructures are also considered as new areas of research for this class of materials.

Chang-Eun Kim received a B.S. degree in the Dept. of Materials Science and Engineering from Yonsei University in 2013. He is pursuing his Ph.D. degree under the supervision of Prof. Aloysius Soon in the same department. His research interests include first-principle description for the phase stability, electronic structure and transport property of narrow-gap semiconductors.

Aloysius Soon holds a Ph. D. in Physics from the University of Sydney, Australia, and joined the Department of Materials Science and Engineering at Yonsei University, Korea, as an assistant professor in 2010. Prior to that, he was an Alexander von Humboldt postdoctoral fellow at the Fritz-Haber-Institut der Max-Planck-Gesellschaft, Germany, under the direction of Prof. Matthias Scheffler. Recently, he was awarded the title of Honorary Research Fellow to pursue joint research at the University of Sydney. His research focuses on the development and application of materials theory and first-principle methods for the fundamental understanding of the chemistry and physics of materials.

Ji-Hwan Lee received a B.S. degree in the Dept. of Material Science and Engineering from Yonsei University in 2013. He is pursuing his Ph. D. degree under the supervision of Prof. Aloysius Soon in the same department. His research interests include density-functional study combined with ab initio thermodynamics of multifunctional interfaces to design a new material system for next-generation energy technology.

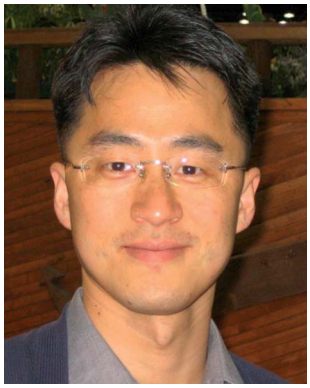

Unyong Jeong received his Ph. D. in Chemical Engineering from POSTECH in Korea. He spent two years as a postdoctoral research associate at University of Washington. He moved to Materials Science and Engineering at Yonsei University in 2006 and now he is an associate professor. His research interest includes production of nanostructured materials, colloids and fibers by electrohydrodynamics, and organic–inorganic hybrid materials for electronic devices. His current interest in the material synthesis is put on the shape control of metal chalcogenides and dimension control of metal nanowires.

Anisotropic MC nanocrystals have predominantly been synthesized in solutions because the size and shape of the nanocrystals can be controlled precisely and the solution-processed printing is an inexpensive way to produce MC films.[40–43] Chalcogens (S, Se, Te) and certain MCs are representative materials having the preferred directional growth. The shape of nanocrystals is known to be dominated by the total minimum surface energy of the crystal facets; this is known as the Gibbs–Wulff theorem.[44] In many chalcogenides, the minimized total surface energies are found in the 1-D shapes because of the asymmetric bond strength. Se and Te are well known to grow into nanowires or nanotubes.[45,46] The layer-structured chalcogenides grow into 2-D nanoplates or nanosheets, as frequently observed in Bi_2Se_3, Bi_2Te_3, MoS_2, and SnS_2, *etc.* Table 1 summarizes the thermodynamic preference in shape and crystal structure of MC nanocrystals. It varies in the metal species and the stoichiometric ratio of the metal to chalcogen (M_xQ_y, M = metal, Q = S, Se, Te). These materials, according to each category, are listed and the tendency to form the anisotropic shape is noted as 'strong' or 'medium' in the table. The preparation of chalcogenides that do not have any preferential growth direction requires purposeful shape-guiding. Normally, the shape of nanocrystals obtained through thermodynamically controlled growth reflects the inherent symmetry of the crystal structure, which is spherical or near spherical due to uniform growth of all crystal facets. Reduction of the surface energy of a certain facet is a powerful way to obtain anisotropic MCs, which can be achieved by selectively attaching organic surfactants or using the organic templates as the shape-determining reactor. The MC nanocrystals can then be merged to form 1-D or 2-D nanostructures. Such oriented attachment can be tailored by engineering the interaction between the nanocrystals. Chemical transformation of pre-existing anisotropic nanocrystals into others has recently received a lot of interest because it allows preparation of nanocrystals that are chemically different, but have the same shape and dimensions. MC nanocrystals reported to date are tabulated (Table 2) according to their synthetic pathways.

This review highlights the common solution-based synthesis of anisotropic MC nanocrystals and the recent advances in applications, with some guidance from first-principle simulations and computations. The synthetic pathways of 1-D and 2-D structures are dealt with in separate sections. We begin with the direct synthesis from organometal precursors and then review the chemical transformation of the premade nanocrystals into others. The Applications section mainly focuses on the research areas which can be practically meaningful in the near future, and then introduces a few emerging topics in physics and chemistry. We conclude this review with discussion on the challenges and future directions of the solution-based synthesis and its applications.

2. Direct synthesis of 1-D chalcogenides

2.1. Intrinsically anisotropic growth

Selenium (Se) and tellurium (Te) inherently grow into anisotropic nanostructures due to the covalent bond in a helical chain along the *c*-axis. The helical chains are hexagonally closely packed through van der Waals interactions. Thus, the stronger atomic bond strength in the *c*-axis results in rapid growth along that direction. Fig. 1A shows the crystal structure of Te with the lattice spacings calculated by the density-functional theory (DFT) with Grimme's van der Waals correction.[47] We performed the DFT calculation within generalized gradient approximation (GGA) for the exchange–correlation functional, given by Perdew, Burke and Ernzerhof (PBE) as implemented in the Vienna *ab initio* simulation package (VASP).[48] The kinetic energy cutoff for the plane-wave basis set is set to 500 eV and the core level interactions are represented by the projector augmented wave (PAW) potentials.[49] From our first-principle density-functional theory (DFT) calculations, we find that the surface energy of the basal plane (normal to the *c*-axis) is indeed relatively higher (0.616 J m^{-2}) than those of the prism planes (~0.463 J m^{-2}), clearly reflecting that cutting the stronger covalent bonds in the *c*-direction involves a larger energetic cost to form those surfaces. Due to this difference in surface energies, the calculated theoretical Gibbs–Wulff shape favors growth along the *c*-axis rather than the *a*- and *b*-axes. This corroborates the fact that selenium nanowires are reported to show a preferential growth

Table 1 Thermodynamic preferences of chalcogenide nanocrystals

	M (metal)	Thermodynamic preference (level)	Crystal structure	Reason	Materials
Q (=S, Se, Te)		1-D (strong)	Trigonal	Chain-like structure	Se, Te
M_2Q	IB	1-D (medium)	Hexagonal	High surface energy in the (0001) plane	Cu_2Q
	IB	0-D (strong)	Cubic	Isotropic surface energy	$Cu_{2-x}Q$
MQ	IIB, IVA	0-D (strong)	Cubic	Isotropic surface energy	ZnQ, CdQ, PbQ
	IIB	1-D (strong)	Hexagonal	High surface energy in the (0001) plane	CdQ, ZnQ
	IVA, VIIIB	2-D (strong)	Orthorhombic	Layered-structure	GeS, GeSe, SnS, SnSe, FeSe, FeTe
MQ_2	IB, IIB, VIIIB	3-D (medium)	Cubic	Isotropic surface energy	FeS_2, CoS_2, NiS_2, CuS_2, ZnS_2
	IVB, VB, VIB	2-D (strong)	Hexagonal	Layered-structure	TiQ_2,ZrQ_2,NbQ_2, TaQ_2, MoQ_2, WQ_2
MQ_3	IVB	1-D (medium)	Monoclinic	Chain-like structure	TiS_3, ZrS_3, $ZrSe_3$, $ZrTe_3$, HfQ_3
M_2Q_3	VA	2-D (strong)	Hexagonal	Layered-structure	Bi_2Se_3, Bi_2Te_3, Sb_2Te_3
	VA	1-D (strong)	Orthorhombic	Chain-like structure	Bi_2S_3, Sb_2S_3, Sb_2Se_3

Table 2 Anisotropic chalcogenide nanocrystals reported to date

Mechanism	Products		Growth	Shape[a]
Intrinsically anisotropic growth	Se, Te, Se_xTe_y		1D	NW,[45,46,54,58,59,61–67] NT,[57,61] NR,[59,60,68] NN,[56] NRB,[53] NB,[57]
	Bi_2S_3		1D	NR[72]
	Sb_2Q_3 (Q = S, Se)		1D	NW[74] NRB[73]
	GeQ (Q = S, Se)		2D	NSt[117]
	FeQ, FeQ_x (Q = Se, Te)		2D	NSt,[121] NF[122]
	SnQ (Q = S, Se)		2D	NSt[119,120]
	MS_2 (M = Ti, Zr, Nb, Ta, Mo), $TiSe_2$		2D	NSt,[127,132,133] ND[126]
	Bi_2Q_3 (Q = Se, Te)		2D	NP,[134,135,222–224] ND[136] NSt,[136] NF[137]
	Sb_2Te_3		2D	NP[138,139,224]
	$Bi_2Te_{3-x}Se_x$		2D	NP[222]
	$Bi_{2-x}Sb_xTe_3$		2D	NP[221,224]
Surfactant driven growth	Cu_2Q (Q = S, Te), $Cu_{2-x}S$		1D	NW,[79]
	PbQ (Q = Se, Te)		1D	NW,[80,82] NR[80,82]
	Sb_2Te_3		1D	NB[83]
	CdSe		2D	NSt,[147] ND[148]
	$Cu_{2-x}Se$		2D	ND[144]
	In_2S_3		2D	NSt[150]
	$NiTe_2$		2D	NF[151]
Oriented attachment growth	PbSe		1D	NR,[95] NW[96]
	ZnQ (Q = S, Se)		1D	NR,[97] NW[98]
	CdQ (Q = S, Se, Te)		1D	NW[92–94,99,108]
	Bi_2Q_3 (Q = Se, Te)		2D	NP[156]
	CdQ (Q = S, Te)		2D	NSt,[155] NP[160]
	PbQ (Q = S, Te)		2D	NSt[157–159]
Chemical transformation	**Reactant**	**Product**		
	Te	M_xTe_y (M = Ag, Cd, Zn, Pb, Bi, Sb, La, Co)	1D	NW,[162,173–177] NT[168–171] NRB[179]
	Te	Ag_2Te–Te–Ag_2Te	1D	Heterostructured NW[178]
	Se	Ag_2Se	1D	NW[66,172,180]
	Ag_2Te	MTe (M = Cd, Zn, Pb)	1D	NW[162]
	CdTe	$PtTe_2$	1D	NT[162]
	CdQ (Q = S, Se)	MQ (M = Pb, Zn)	1D	NR[181,182]
	Ag_2Se	CdSe	1D	NW[66,180]
	$Cd(OH)_2$	CdE (E = S, Se, Te)	1D	NT[184,185]
	$LiMo_3Se_3$	Au, Ag, Pt, Pd	1D	NW[188]
	Te	Pt, Pd	1D	NT,[189] NW[189]
	Ti_2S	Cu_2S, CdS	2D	Toroid[183]
	SnSe	SnTe	2D	NSt[186]

[a] Abbreviations are as follows: nanowire (NW), nanorod (NR), nanotube (NT), nanobelt (NB), nanoneedle (NN), nanoribbon (NRB), nanowire bundle (NWB) for 1D nanostructures, and nanoplate (NP), nanosheet (NSt), nanodisc (ND), and nanoflake (NF) for 2-D nanostructures.

along the [001] direction in a wet chemical process.[50] The 1-D growth of this system is also attributed to the minimization of the area of facets (*i.e.* basal planes) with relatively high surface energies, lowering the total free energy of the system. But in a dry vapor–solid process with relatively high temperature (~950 °C), the seed effect was found to be more dominant in the growth of nanowires.[51]

Considerable effort has been devoted to generate diverse 1-D Se and Te nanostructures by solution-based synthesis.[52–66] Yu and co-workers synthesized *t*-Te nanowires 4–9 nm in diameter and hundreds of micrometers in length using hydrothermal methods (Fig. 1B and C).[67] HR-TEM images clearly showed that the *t*-Te nanowires grew predominantly along the *c*-axis. Because Se and Te can form a solid solution on the basis of the Hume-Rothery rule, binary Se_xTe_y alloys also tend to grow favorably along the *c*-axis, allowing the formation of Se_xTe_y and Se_xTe_y@Te core–shell nanorods.[68,69]

Pnictogen chalcogenides, M_2Q_3 (M = Bi, Sb; Q = S, Se, Te), are nanocrystals with a highly anisotropic crystal structure. Pnictogen chalcogenides have been extensively investigated because of their promising thermoelectric and optoelectronic properties. Interestingly, in addition to their 2-D structures, Bi_2S_3, Sb_2S_3, and Sb_2Se_3 possess a strong tendency to grow along the *c*-axis into a 1-D nanostructure. Such tendency is attributed to the chain-like molecular conformation that results from V–VI bonding and van der Waals interactions between the chains (Fig. 1D). This anisotropic growth mode may, once again, be accounted for on thermodynamic grounds, referring to their surface Gibbs free energy differences between different surfaces. This is illustrated using the orthorhombic Bi_2S_3 as an

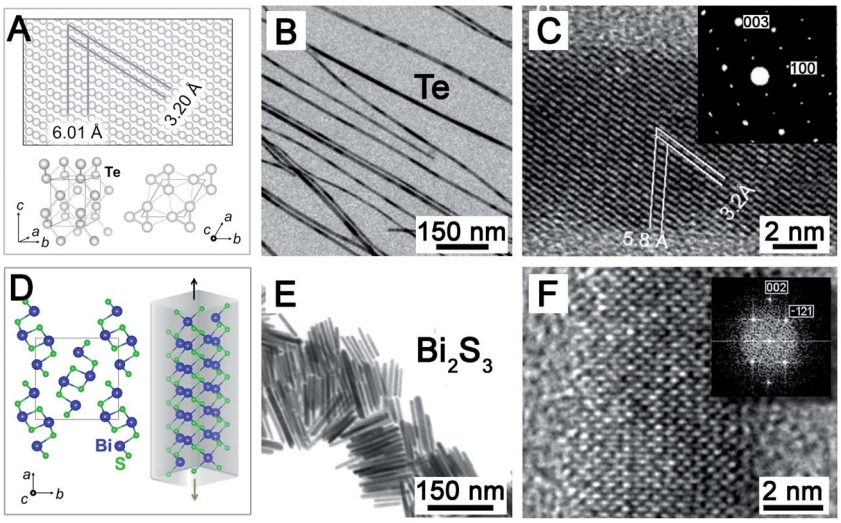

Fig. 1 Intrinsic anisotropic growth of 1-D Te, Bi_2S_3 nanocrystals. (A) Tellurium (Te) crystal structure viewed along the *a*-axis, while the insets show perspective and top views of the unit cell. Lattice spacings were obtained from the density-functional theory (DFT) calculations with Grimme's van der Waals correction. The projector augmented wavefunction method (PAW) was used for core level potential, while the PBE-GGA exchange correlation functional is used. (B) TEM and (C) HR-TEM images of *t*-Te nanowires and the electron diffraction (ED) pattern appears as an inset.[67] Adapted with permission from ref. 67, Copyright American Chemical Society. (D) Crystal unit cell of Bi_2S_3 viewed along the *c* axis, [001] direction. The growth direction is noted with arrows along the *c*-axis. (E) TEM and (F) HR-TEM images of Bi_2S_3 nanorods with an ED pattern (inset in F).[71] Adapted from ref. 71 with permission from Wiley VCH.

example. Using first-principle DFT calculations, it was shown that the surface free energy of the (001) surface of Bi_2S_3 (0.423 J m^{-2}) was higher than those of other low-index surfaces.[70] Two other low index facets—(100) and (010) facets (0.359 J m^{-2} and 0.349 J m^{-2}, respectively)—had slightly different surface energies, but were both similarly lower than that of (001). Thus, to afford the minimization of the free energy of the system during growth, Bi_2S_3 is thermodynamically driven to conform to a crystal morphology (*i.e.* a rod-like shape) which minimizes the area of the (001) facet, while maximizing that of the other two facets. A schematic of this equilibrium crystal shape of Bi_2S_3 is shown in Fig. 1D.

In numerous experimental studies, Bi_2S_3 nanorods were synthesized through a hot injection method with elemental sulfur, bismuth chloride, and oleylamine.[71] Bismuth chloride dissolved in oleylamine was first transformed into BiOCl, then further reduced into elemental bismuth by the amine groups when the solution was heated up to 170 °C. Uniformly sized Bi_2S_3 nanorods were produced by rapid hot injection of a sulfur solution. The as-synthesized Bi_2S_3 nanorods were single crystals that showed preferential growth along the [001] direction (Fig. 1E and F). If some form of kinetic hindrance occurs during the reaction, the final shape of nanocrystals may deviate from the ideal one-dimensional morphology, *e.g.* partially generating quasi-two-dimensional crystals as the kinetic shape. This could then explain the experimental observation in the growth of Bi_2S_3 nanowires, where small portions of nanoplates were grown together with thin and long nanowires.[72] This delicate difference in the relative surface free energy of the various prism facets of Bi_2S_3 can be used to tailor and design the desired morphology for its specific application. Sb_2S_3 and Sb_2Se_3 favorably crystallized into nanorods with an orthorhombic crystal structure.[73] Zheng and co-workers reported the hydrothermal synthesis of 1-D Sb_2Se_3 nanostructures with controlled aspect ratios.[74] Short nanorods were produced at high temperatures (150 °C), which is due to rapid exhaustion of the sources (Sb^{3+} and Se^{2-}) and sequential lack of driving force for nucleation and growth into nanowires. Thick, long nanorods were prepared at high concentrations by a continuous reaction between Sb^{3+} and Se^{2-}. The diameter of the nanowires slightly increased with the prominent increase of the length until the sources were consumed completely.[74]

2.2. Growth by surface energy control

During thermodynamic growth of nuclei, the fastest growing facets should disappear eventually due to the increased surface energy, while the slowest growing facets should survive as the final planes of the product. Controlled growth of nanocrystals with anisotropic morphologies has been extensively investigated by adjusting organic surfactants over the past two decades. Although MC nanoparticles with diverse asymmetric shapes had been experimentally achieved by controlling the surface energies, the interactions between organic molecules and specific facets are still not clearly understood. This surface energy minimization possibly enables evolution into 1-D nanostructures in a way that the specific binding of surfactant molecules to a preferred facet reduces the surface energy of the plane. First principle electronic structure simulation revealed the effect of organic surfactant binding on the various surfaces of a CdSe crystal.[75,76] The typical capping agents include phosphonic acids (PA), phosphine oxides (PO), trimethylamines (TMA), and carboxylic acids (CA). The (0001), (000$\bar{1}$), (01$\bar{1}$0), and (11$\bar{2}$0) facets were selected and systematically examined on the

effect of binding energy with ligands. Fig. 2A shows the configurations of the PO and PA bound to the four facets of $Cd_{33}Se_{33}$ dots. The energy was stable when Cd or Se atoms made bonds with the oxygen double bonded to the phosphor (PO and PA) or the carbon (CA). For TMA molecules, the binding took place between Cd or Se atoms and the lone pair electrons on the nitrogen atom. Binding energies between the surfactant molecules and the facets of Cd_xSe_x ($x = 15, 33$) were calculated (Table 3). PO and PA were found to bind more strongly to the nonpolar side facets with Bravais indices $(01\bar{1}0)$ or $(11\bar{2}0)$ than to the polar surfaces (0001) and $(000\bar{1})$. The preference in binding facets indicates faster growth of polar facets than the nonpolar facets for reducing the total surface energies of the resulting nanostructures. For polar facets, the binding energies of these surfactants to the (0001) surface were much smaller than those to the $(000\bar{1})$ surface, indicating that the growth of CdSe along the *c*-axis would be dominated by the Se-terminated (0001) facet. In many experimental synthesis reactions, CdSe spheres have been produced in the presence of CA surfactants,[77] which is attributed to the small and weak binding energies of CA on the CdSe surfaces. Unlike other surfactants, trimethylamine (TMA) binds slightly stronger to the Se-terminated (0001) facets, which can induce the faster growth of Cd-dominated $(000\bar{1})$ along the *c*-axis.

The crystal structures could be engineered by surfactant molecules through fine-tuning of surface energies. Generally, wurtzite is a thermodynamically stable crystal structure for both CdS and CdSe in bulk states. The metastable zinc blend phase has been mainly allowed at low reaction temperature (<240 °C) or in small size limit (<4.5 nm). Indeed, zinc blend CdS nanowires with 15 nm diameter could be successfully synthesized even at high reaction temperature (310 °C). Theoretical analysis confirmed that trioctylphosphine (TOP) molecules are likely to bind strongly to the (001) surface of the zinc blend CdS than to the surfaces of the wurtzite CdS (Table 3).[78] In some cases, a mixture of surfactants can effectively direct 1-D growth. Ultrathin (1.7 nm) hexagonal Cu_2S nanowires as long as tens of micrometers were successfully synthesized using a mixture of dodecanethiol (DT) and oleic acid (OA) as the solvent.[79] DT served as the primary capping ligand for nanowire growth through the formation of thiol-to-Cu(I) bonding on the surface. The growth of Cu_2S nanowires could be attributed to the synergistic effect of the solvent OA and the adsorbent affinity of DT.

The energy decrease of the target facet by the organic surfactant is often not large enough to guide the growth to a 1-D nanostructure. In this case, use of an organic template whose molecules form complexes with the inorganic sources can be a powerful way to generate anisotropic nanocrystals.[80–82] Due to the preferential bonding of the organic molecule to a specific inorganic element, the inner surface of the template is covered by the preferred element. The reduced atoms are stabilized by the complex molecules and nuclei are initiated at the inner surface of the template. Consecutive assembly of the inorganic elements in a 1-D template facilitates the growth into nanowires. Ma and co-workers demonstrated that PbTe can be synthesized into nanowires and nanorods in the presence of sucrose templating molecules.[82] Normally, PbTe grows thermodynamically into spherical or cubic nanoparticles due to its preferred isotropic cubic crystal structure. The key factor in

Table 3 Binding energies (in eV) calculated for various ligands to the surfaces of CdE (E = S, Se) crystals. The energies marked with "a" and "b" were calculated from the $Cd_{15}Se_{15}$ and $Cd_{33}Se_{33}$ clusters, respectively. The elements (Cd, Se, S) placed beside surface notations represent the element terminated at the surfaces[a]

Ligand	$(000\bar{1})$Cd	(0001)Se	$(01\bar{1}0)$	$(11\bar{2}0)$
Wurtzite Cd_xSe_x [ref. 75]				
PO	1.06a/0.85b	0.66a/0.63b	1.23b	1.37b
PA	1.12a/1.11b	0.66a/0.67b	1.45b	1.26b
CA	0.68a	0.42a	—	—
TMA	0.91a	1.05b	—	—
Wurtzite CdS [ref. 78]				
	(0001)S	(0001)Cd	$(10\bar{1}0)$	$(11\bar{2}0)$
TOP	3.25	0.50	0.50	0.50
OA	3.75	0.50	0.75	2.65
Zinc blend CdS [ref. 78]				
	(001)	(111)S	(111)Cd	(110)
TOP	3.65	1.30	0.50	0.20
OA	3.20	0.3	0.15	1.60

[a] Abbreviations of the ligands are as follows: phosphine oxide (PO), phosphonic acid (PA), carboxylic acid (CA), trimethylamine (TMA), trioctylphosphine (TOP), and oleic acid (OA).

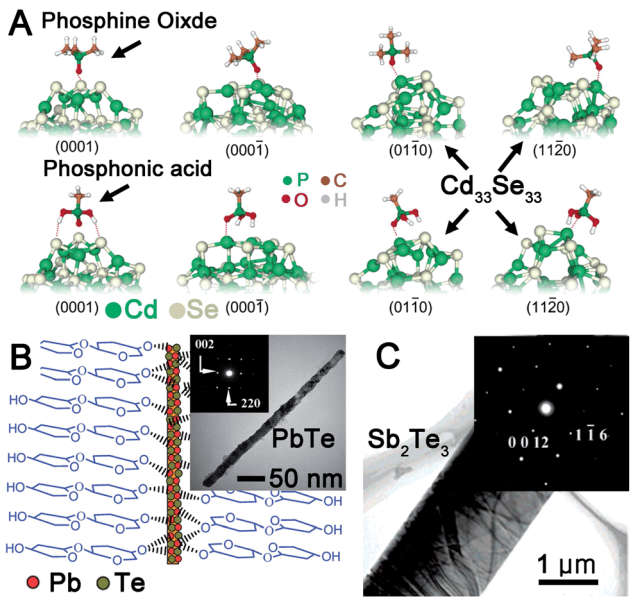

Fig. 2 (A) Calculated geometries of phosphine oxide and phosphonic acid bound to the four facets of a $Cd_{33}Se_{33}$ cluster.[75] (B) Schematic showing the growth mechanism of PbTe nanowires in the presence of sucrose with TEM images and the corresponding ED pattern as an inset; anisotropic growth is due to the selective binding between the hydroxyl group sucrose and Pb atoms.[82] (C) TEM image of a single Sb_2Te_3 nanobelt with the SAED pattern (inset in C).[83] Adapted from ref. 75, 82, and 83 with permission from American Chemical Society.

promoting the 1-D growth was the addition of sucrose, which has hydroxyl groups that interact exclusively with Pb (Fig. 2B). In addition, the π–π electron interactions of sucrose served as an organic template for the growth of nanowires. PbTe nanocubes and flower-shaped clusters were synthesized under the same conditions when sucrose was replaced by other typical surfactants such as trioctylphosphine (TOP) and trioctylphosphine oxide (TOPO). Selective interactions between the hydroxyl groups and Pb atoms were confirmed by replacing Pb with Pt in the same synthesis process. The Pt source caused the formation of highly agglomerated randomly shaped PtTe crystals under the same experimental conditions. This result suggests the lack of effective interactions between sucrose and both elements (Pt, Te). PbTe nanowires with a thickness of 10–16 nm and a length of 400–600 nm were obtained in the presence of sucrose by injecting precursors into a pentanediol solvent heated at 210 °C.

This templating approach is a promising way to synthesize diverse MC nanocrystals. However, several factors determining the shape of the nanocrystals are mingled; the effect of the reduction rate of the precursors, the change of dipole according to the solvent in use, the stability and thermodynamic shape of the template under the synthesis conditions, and so on. Hence, weak complexation between the source element and surfactant molecules may not be large enough to generate stable templates. In this case, the use of the ionic surfactants can be a noticeable approach to produce anisotropic nanocrystals. The molecules containing ionic charges exist in the forms of vesicles or micelles when their concentration is over a critical value. Zhang and coworkers successfully synthesized Sb_2Te_3 nanobelts with a length of several tens to hundred micrometers in the presence of an anionic surfactant, sodium bis(2-ethylhexyl)sulfosuccinate (AOT).[83] The pnictogen chalcogenides such as Bi_2Se_3, Bi_2Te_3, and Sb_2Te_3 have been known to preferentially form 2-D anisotropic crystal structures. However, the AOT molecules suppressed the growth along the *a*- or *b*- axes of the Sb_2Te_3 crystals and formed 1-D templates in which the growth of the crystals is confined. In the absence of AOT, irregular 2-D nanoplates were obtained under identical reaction conditions (Fig. 2C). Ionic surfactant AOT has also been used for controlled synthesis and evolution of ZnS nanowires with diameters of 30 nm and lengths up to 2.5 μm.[84] At specific AOT concentration, a rod-like micelle of AOT acts as a template for the formation of ZnS nanowires. Zn–thiourea complexes may undergo slow decomposition to produce nanowires in the micelle templates. The same group has also produced ZnSe nanorods using the AOT micelle-template.[85]

2.3. Axial growth by oriented attachment of nanocrystals

Classically, crystals have been considered to grow through (i) spontaneous growth of nuclei by consecutive atomic addition or (ii) dissolution of unstable small particles followed by reprecipitation onto more stable particles. The latter concept, the so-called Ostwald ripening process, is based on the solubility difference explained by the Gibbs–Thompson equation.[86,87] The ripening process has been used to explain particle coarsening, but cannot fully explain the crystal growth behavior or the shape evolution.[88] Since Penn and Banfield first pioneered the oriented attachment as a new crystal growth mechanism,[89–91] several anisotropic growth mechanisms of MC nanocrystals including CdTe, CdSe, CdS, PbSe, ZnS, and ZnSe, have been explained.[92–99] The oriented attachment refers to the direct self-organization of two particles into a single crystal caused by sharing a common crystallographic orientation. A large single crystal can form through consecutive attachment of the small nanocrystals, which is different from the simple physical assembly of nanomaterials (which we will discuss later). Because the oriented attachment involves the assembly of nanocrystal building blocks, tailoring the way of attachment generates 1-D or 2-D structures with tunable properties. The driving force of this attachment is removal of the high-energy surfaces.[88] As particles approach one another in solution, they are assembled by additional energy between the surfactants (van der Waals interactions or dipole interactions). When the areal density of the capping agent on high energy surfaces is low or negligible, the surfaces meet each other and form long nanowires or nanobelts (Fig. 3A). The defects such as misorientation and stacking faults are caused by the direct coagulation of the nanocrystals.[100,101] After coalescence, the nanocrystals are thought to rearrange into a particle with identical crystallography, which raises the possibility of transformation into a large single crystal.[102,103] The epitaxial rearrangement takes place through relaxation of the stress caused by misorientation at the attachment interface. However, the growth *via* the ripening process can occur simultaneously along

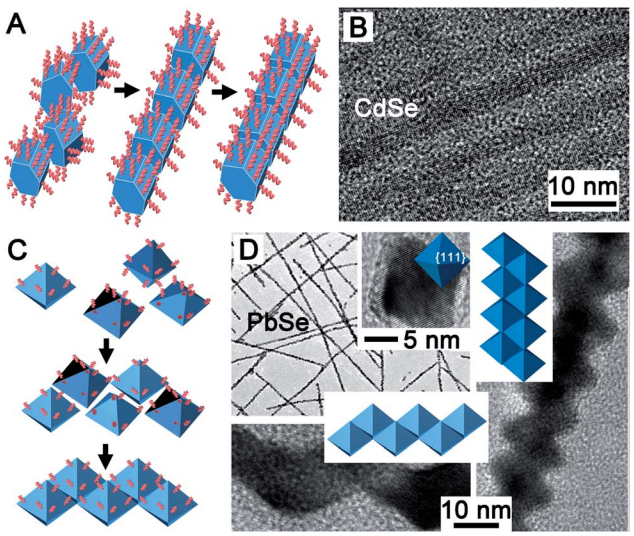

Fig. 3 Axial growth by oriented attachment of CdSe, PbSe nanowires. (A) Schematic illustration showing each growth stage during morphology evolution of CdSe quantum wires. (B) HR-TEM image of CdSe nanowires.[108] Adapted from ref. 108 with permission from IOP publishing. (C) Schematics of segments showing the assembly and growth of octahedral PbSe nanocrystals into zigzag nanowires. (D) TEM and HR-TEM images of octahedral repeat unit and zigzag nanowires depending on the two attachment modes.[96] (Schemes show the different attachment modes of octahedral PbSe nanocrystals.) Adapted from ref. 96 with permission from American Chemical Society.

orientated attachment. Theoretical and experimental studies have demonstrated that strong surface adsorption of capping ligands to a specific facet can hinder growth *via* the ripening process and facilitate pure oriented growth.[104–106] Surface adsorption of anions was confirmed to slow down the ripening process because the anions were able to effectively restrict the dissolution of particles in solution.[107]

Barnard and co-workers have demonstrated experimentally and theoretically that the growth of CdSe nanowire is based on the oriented attachment rather than the continuous axial growth of nanorods (Fig. 3A and B).[108] CdSe nanowires were synthesized by reacting cadmium acetate (CdAc2) and selenourea in an alkylamine solution (octylamine or oleylamine). The synthesis involved three different growth stages: (i) the formation of initial nanocrystals, (ii) formation of pre-wire aggregates with the configuration of a string of pearls, and (iii) structural transformation into single-crystal nanowires by thermally annealing the pre-wire aggregates. The pre-wire aggregates whose thickness was similar to the diameter of nanocrystals could be interpreted as the key evidence of the oriented attachment. The oriented attachment was described with a thermodynamic model based on the Gibbs free energy. The total free energy G is described in terms of surface energy (γ) weighted by the factor f (such that $\sum_i f_i = 1$),

$$G = \Delta G_f^0 + \frac{M}{\rho}(1-e)q\sum_i f_i\gamma_i \quad (1)$$

where ΔG_f^0 is the standard free energy for the formation of bulk materials, M is the molar mass, ρ is the density, q is the surface to volume ratio, and e is the volume dilation induced by the surface stresses σ_i. Details about the assumptions and simplification can be found in ref. 108. According to the thermodynamic model and first-principle calculations, CdSe basically prefers to grow as short nanorods (aspect ratio: 2–4), indicating that the thermodynamic axial growth by consecutive atomic addition is not a dominant formation mechanism. Furthermore, kinetically controlled axial growth alone was also proved not to be a dominant mechanism from the calculation of the nucleation probability on the surfaces of the CdSe nanorods. The growth along the $\langle 0001\rangle$ direction *via* attachment of (0001) facets was the most, energetically, stable for the growth of CdSe nanowires.

Murray and co-workers synthesized nearly defect-free and highly uniform PbSe nanowires *via* the oriented attachment.[96] By tailoring reaction conditions, nanowires with diverse shapes were prepared such as straight, zigzag, helical, branched, and tapered nanowires. Attachment of the {100}, {110}, or {111} facets was dependent on the chemical nature of the surfactant(s) used in the synthesis. In the presence of oleic acid only or the co-surfactants of oleic acid and *n*-tetradecylphosphonic acid (TDPA), nanocrystals assembled along the $\langle 100\rangle$ axis, which was attributed to faster growth of the {111} facet than the {100} facet. Dipole moment along the $\langle 100\rangle$ axis aligned the nanocrystals into nanowires. By replacing TDPA with long, aliphatic primary amines (dodecylamine, hexadecylamine (HDA), oleylamine, *etc.*), octahedral PbSe nanocrystals containing eight {111} facets formed preferentially due to selective blocking of the {111} facets by the binding of amines. Two types of zigzag nanowires were obtained depending on the attachment mode of the octahedron nanocrystals (Fig. 3C and D). Helical nanowires formed when HDA and oleic acid were used as co-surfactants in the reaction medium of trioctylamine. Although PbSe crystals have a highly symmetric cubic structure, oriented attachment leads to successful synthesis of PbSe nanowires with the same crystal structure. The concept of dipole–dipole interactions as a driving force directing 1-D nanostructures has been proposed previously.[92] In a subsequent study, Murray and co-workers reported the formation of PbSe/PbS core–shell heterostructures using the pre-formed PbSe nanowires as the building blocks.[109]

Highly uniform nanocrystals can assemble to form superstructures with regular particle–particle distances. Self-assembly of the nanocrystals is governed by the attractive forces between the nanocrystals such as van der Waals, Coulombic, and dipole–dipole interactions. It is, currently, not under precise control whether the nanocrystals evolve into a superstructure by the physical self-assembly or grow into a single crystal by the oriented attachment. One of the key factors inducing the oriented attachment is the control of the degree of passivation of target surfaces with organic surfactants. The others include solvent species, reaction temperature, and concentration of nanocrystals. These interactions are often entangled, which makes it difficult to predict the product. Directed alignment of nanocrystals by external forces may help the oriented attachment process. Alignment of anisotropic nanoparticles is challenging because the interaction between anisotropic nanocrystals is direction-dependent, typically causing raft-like assembly with short range ordering.[110–112] In the presence of an external electric field, the MC nanorods are forced to align along the E-field.[113–115] Russell and co-workers reported 'self-corralling' of CdSe nanorods under an applied electric field.[116] The permanent dipole moment and inherent dielectric properties of CdSe nanorods enhanced the alignment of nanorods along their long axis, parallel to the field. This alignment followed by epitaxial merging of the nanocrystals may enable the preparation of long single-crystal nanowires, which may allow the fabrication of aligned nanowires on a substrate.

3. Direct synthesis of 2-D chalcogenides

3.1. Intrinsically anisotropic 2-D growth

The shape of nanocrystals is dominated by the surface energy of the facets. For some MCs, 2-D shapes (nanoplates, nanodiscs, nanoflakes, nanosheets) are thermodynamically favored. Examples include the VA–VIA (GeS,[117] GeSe,[117] SnS,[118,119] and SnSe[120]), VIIIB–VIA (FeSe[121,122] and FeTe[121]), IVB–VIA (TiQ_2,[123–127] ZrQ_2, and HfQ_2, Q = S, Se, Te[123,124,126,128]), VB–VIA ($NbSe_2$ (ref. 126 and 129) and $TaSe_2$ (ref. 126 and 130)), VIB–VIA (MoS_2, $MoSe_2$, WS_2, and WSe_2 (ref. 131−133)), and VA–VIA (Bi_2Se_3, Bi_2Te_3, and Sb_2Te_3 (ref. 134−139)). The structural preferences of the materials listed above have been confirmed by theoretical

studies[123,140] and vapor-phase synthesis[141–143] which has no surfactant-driven effect. The basic crystal structures of the metal chalcogenides are illustrated in Fig. 4. They commonly assume the chemical stoichiometries of MX_2 or M_2X_3, where M is the metal and X is the chalcogen. In these structures, the M atoms are often 6-fold coordinated (octahedral distortion occurs when M is a VB or VIB metal atom; see Fig. 4A, B and D), while the X atoms are 3-fold coordinated (and also 6-fold in the case of M_2X_3; see Fig. 4C). Due to this unique structuring, the 3-fold coordinated X chalcogenide ions form localized pairs of electrons, frequently leading to the formation of van der Waals-bonded layered structures, exposing X-terminated layers. Metal chalcogenides may occasionally take on the MX stoichiometry and assume the distorted B1 structure (Fig. 4E). These metal chalcogenides are characterized by a MX stoichiometric bi-layered structure, weakly bonded by van der Waals forces.

In solution-based synthesis, the use of surfactants to prevent aggregation of nanocrystals affects the thermodynamic preference and often generates unexpected structures. Jeong and co-workers recently reported a surfactant-free synthesis of Bi_2Te_3 and Bi_2Se_3 nanoflakes in a gram scale (Fig. 5).[137] Formation of the 2-D nanocrystals in the absence of any surfactant is a strong evidence of the preference in the growth direction. The layered crystal structures of bismuth chalcogenides are illustrated in Fig. 5A. Five successive atomic planes [$Te_1(Se_1)$–Bi–$Te_2(Se_2)$–Bi–$Te_1(Se_1)$] constitute one quintuple along the *c*-axis. Basically, bismuth chalcogenides preferentially grow into 2-D nanostructures because of weak van der Waals interactions between adjacent $Te_1(Se_1)$ atomic planes that confer bismuth chalcogenides with an intrinsically anisotropic bonding nature. Because the top and bottom surfaces which consist of Te or Se atoms are not stabilized by the surfactant, secondary nanoplates grow vertically, as shown in Fig. 5B and D. Clear lattice fringes are visible in the HR-TEM images shown in Fig. 5C (Bi_2Te_3) and Fig. 5E (Bi_2Se_3) and the corresponding fast Fourier transform (FFT) patterns demonstrate the single crystalline nature of the nanoplates. The cross-section of the Bi_2Se_3 nanocrystals (Fig. 5F) indicated 6 quintuple thickness.

As long as the agglomeration is avoided or the aggregates are redispersed in solution by ultrasonic treatment, synthesis of the surfactant-free 2-D nanocrystals deserves further investigation. The layer-structured MCs have a high chance of success to be produced in the absence of a surfactant. In most layered MCs, stacking of the atomic layer ends typically with the negatively charged chalcogen atoms or the positively charged metal atoms. Depending on the metal species and crystal structure, the uniform direction of the dipoles over the large basal planes provides better colloidal stability compared to the isotropic particles. A small amount of inorganic chalcogenide ligands may greatly enhance the colloidal stability in polar solvents. Recently, Talapin and coworkers found that various molecular metal chalcogenide complexes (MCCs) such as $[Sn_2S_6]^{4-}$ and $[Sn_2Se_6]^{4-}$ could serve as convenient ligands for colloidal nanocrystals.[144] The surface inorganic surfactants greatly facilitate charge transport between individual nanocrystals.[145] The insulating organic surfactants of the typical 2-D nanocrystals diminish the unique properties of the 2-D nanocrystals such as high electron mobility and topological insulation. The inorganic ligands may allow the use of solution-based 2-D MCs as the semiconducting active layer for future electronic devices.

3.2. Surfactant-driven growth of 2-D nanocrystals

2-D growth of MCs that does not form a layered structure is a challenging subject because of the lack of a driving force for anisotropic growth. As in the case of 1-D growth, 2-D chalcogenide nanostructures can be obtained *via* surfactant-driven growth. In addition to lowering the surface energy of specific

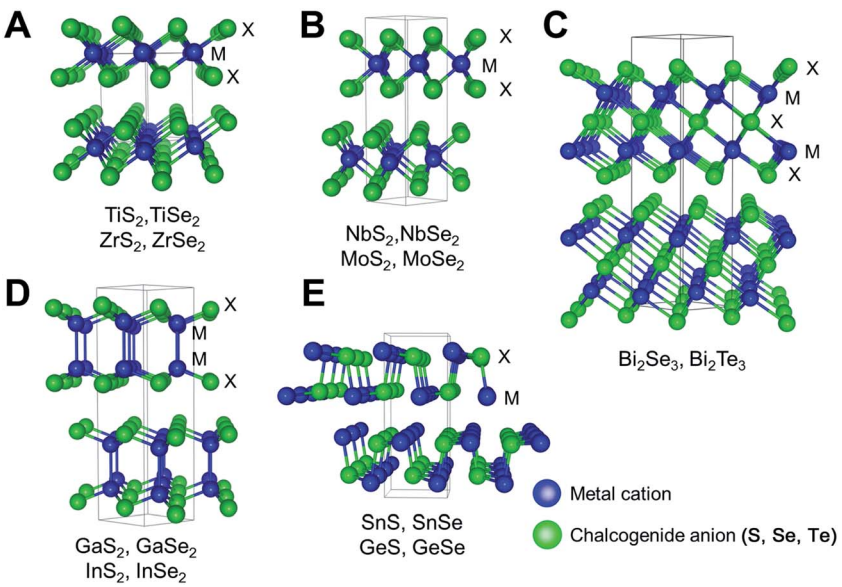

Fig. 4 Crystal structures of various MC layered materials: Schematic descriptions of various metal chalcogenide crystals with layered geometry with stoichiometries MX_2 (in A, B, and D), M_2X_3 (in C), and MX (in E).

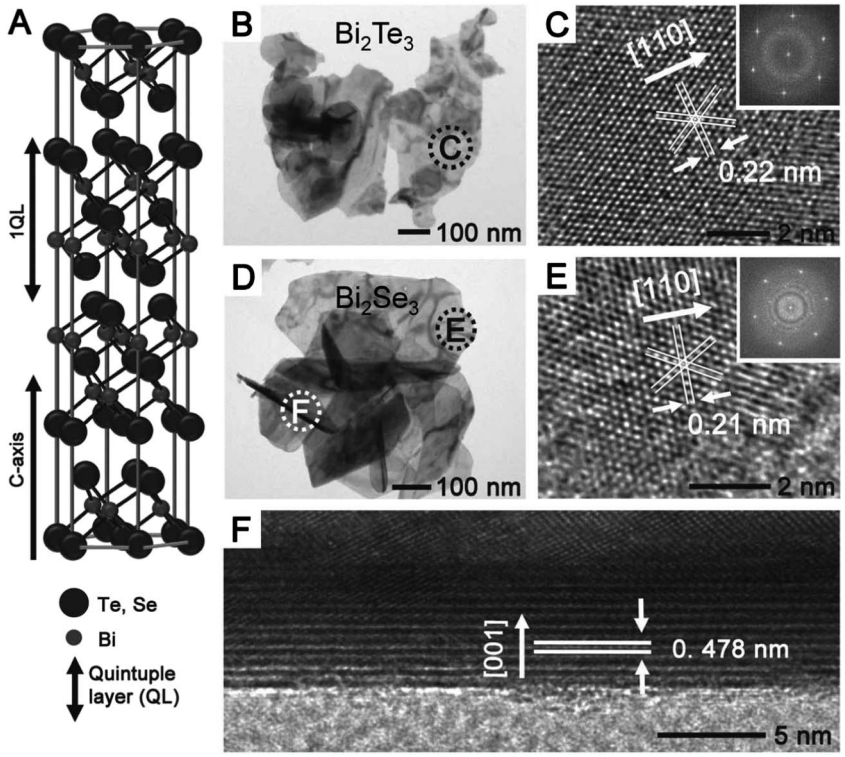

Fig. 5 (A) Layered structure of bismuth chalcogenides (Bi_2Te_3, Bi_2Se_3). Five consecutive atomic planes [$Te_1(Se_1)$–Bi–$Te_2(Se_2)$–Bi–$Te_1(Se_1)$] consisting of one quintuple layer along the *c*-axis. (B) TEM image of as-synthesized Bi_2Te_3 nanoflakes and (C) HR-TEM image of the area designated by the letter C in panel B. (D) TEM image of as-synthesized Bi_2Se_3 nanoflakes and (E) A HR-TEM image of the area indicated by the E in panel D. (F) HR-TEM image showing a side view of the Bi_2Se_3 nanoflake indicated by the letter F in panel D. The insets in C and D are the corresponding FFT patterns.[137] Adapted from ref. 137 with permission from Wiley VCH.

facets, surfactants can serve as soft templates for 2-D nanocrystals. For example, the hexagonal wurtzite crystals normally grow isotropically into 0-D nanocrystals or into 1-D nanowires because the (0001) facet has the highest surface energy.[146] Recently, Hyeon and coworkers succeeded in preparing lamellar-structured CdSe nanosheets as thin as 1.4 nm.[147] They employed a soft colloidal template method, in which organic layers consisting of cadmium chloride and alkyl amine complexes functioned as 2-D templates to generate CdSe nanosheets. In a zinc blend cubic structure, polar axes along the ⟨111⟩ or ⟨001⟩ direction usually facilitate 1-D nanocrystal growth. Such dipole moments exist at the alternating layers of Cd and Se elements. Recently, Peng and co-workers synthesized CdSe 2-D quantum disks (1–3 nm in thickness) with a zinc blend crystal structure.[148] The 2-D CdSe quantum disks were synthesized by suppressing the growth along the polar axes. More specifically, basal planes with exposed layers of Cd ions were passivated by the negatively charged carboxylate groups of the deprotonated fatty acid ligands, thereby neutralizing the dipole from the Cd ions. The close packing of the hydrocarbon chains of the fatty acids enabled the 2-D growth of CdSe nanocrystals. Various 2-D chalcogenide nanocrystals with non-layered structures have also been prepared using a similar synthetic route, including $Cu_{2-x}Se$ nanodiscs,[149] In_2S_3 nanosheets,[150] and $NiTe_2$ nanoflakes.[151] Dubertret and co-workers extended this strategy to synthesize CdSe/CdS and CdSe/CdZnS core–shell nanoplatelets.[152] They first synthesized zinc blend CdSe nanoplatelets capped by carboxylate ligands,[153] and exchanged the ligand by dodecanethiol without disrupting the shape of the thin nanoplatelets. Layer-by-layer deposition of S and Cd enabled CdS coating with a controllable shell-thickness.

The organic surfactants can serve as a carbon source during high temperature sintering. Very recently, carbon-coated FeS nanosheets with lateral lengths of 100–200 nm and thicknesses of 4–10 nm have been prepared by surfactant-assisted solution-based synthesis.[154] The governing factor in controlling the morphology of the FeS nanocrystals was the shape of the micelle directed by 1-dodecanethiol (DDT). DDT was used as both the sulfur source and the surfactant to produce the 2-D FeS nanostructures. At a high concentration of DDT (molar ratio of $Fe(acac)_3$: DDT = 1 : 20), an Fe–DDT complex with a lamellar structure was formed in an oleylamine solution. The complex served as a soft template for the nucleation and growth of the FeS nanosheets. Spherical micelles of an Fe–DDT complex were formed at a lower concentration of DDT (1 : 4); hence polycrystalline nanoparticles of FeS were produced. The hydrocarbon tails of DDT at the surfaces of the nanosheets turned into an amorphous carbon layer after sintering at 400 °C under a nitrogen atmosphere, resulting in the formation of carbon-coated FeS nanosheets.

Surfactants can tweak the growth conditions for further fine-tuning of the 2-D growth regime. The effects of surfactants on

the synthesis of ultrathin (~4 nm) Bi_2Se_3 nanodiscs and nanosheets have recently been investigated (Fig. 6).[136] Bi_2Se_3 grew faster laterally and the basal planes were covered with negatively charged Se atoms. When a negatively charged surfactant, poly(acrylic acid) (PAA), was used, flower-like nanocrystals were obtained, which were similar to the surfactant-free products. In contrast, well-defined Bi_2Se_3 nanodiscs were obtained in the presence of a weakly positive polymer surfactant, poly(vinylpyrollidone) (PVP). The effect of surfactant charge on the 2-D shape formation was examined by mixing PVP and poly(ethylene imine) (PEI) as co-surfactants at different molar ratios: 10 : 0 (Fig. 6A and B), 9 : 1 (Fig. 6C), 8 : 2 (Fig. 6D), 3 : 7 (Fig. 6E), and 0 : 10 (Fig. 6F). Binding of the positively charged primary amines to the basal plane was much stronger than that of the tertiary amines in PVP. As the molar ratio of PEI increased, the surface energy of the basal plane decreased, resulting in wide nanosheets with the thickness of the nanodiscs maintained. This effect of surfactant charge was utilized to synthesize various 2-D MCs in the form of nanoplates and nanosheets. Sb_2Te_3 hexagonal nanoplates have been synthesized using both solvothermal[138] and hydrothermal approaches.[139]

3.3. Formation of 2-D nanocrystals by lateral attachment

Although oriented attachment is a relatively new synthetic route, recent advances have proven that this strategy can be used to generate diverse 2-D MC nanocrystals.[155–160] Preparation of the 2-D MC nanocrystals by the oriented attachment is relatively easier than the formation of 1-D nanocrystals by the same approach. The layer-structured MCs tend to expose chalcogen atoms on the top and bottom surfaces of the nanocrystals. Thus, passivation of those surfaces can be selectively achieved even with weakly binding surfactants rather than that of the side surfaces. Growth into nanoplates or nanosheets is energetically favorable due to the reduced surface energy on the top and bottom surfaces. The side surfaces with a higher energy should be the active sites leading to the oriented attachment. This oriented attachment is expected to be more effective when the thickness of the nanocrystals is small and the binding of surfactants to the top and bottom surfaces is strong.

The time-dependent shape evolution during the lateral oriented attachment has been observed in several 2-D MC nanocrystal systems.[136,161] For example, single-crystalline SnSe nanosheets with a thickness of ~1 nm and a width of ~300 nm are synthesized by heating a mixture solution of SeO_2, $SnCl_4 \cdot 5H_2O$, oleylamine, and 1,10-phenanthroline (Phen) at 120 °C followed by aging at 260 °C for 30 min. The TEM studies visualized the growth process which included nucleation of SnSe nanocrystals, aggregation of the nanocrystals into 2-D polycrystalline pseudo-sheets, and transformation of the pseudo-sheets into single-crystalline nanosheets. This growth mechanism was consistent with the result demonstrated by Schaak and co-workers.[120] In their synthesis, 1,10-phenanthroline (Phen) played a vital role as a capping agent in determining the formation of SnSe nanosheets. In an early stage, Phen bound strongly to the basal plane of the newly formed SnSe nanosheets in cooperation with oleylamine, which suppressed the vertical growth of nanosheets. In the absence of Phen, 3-D SnSe nanoflowers were obtained because the stabilization of the basal plane by oleylamine molecules was insufficient to prevent the second growth of SnSe nanoplates on the basal planes.

Weller and co-workers utilized this strategy to synthesize PbS nanosheets from PbS nanoparticles[158] (Fig. 7). They based their approach on the standard synthetic protocol used to prepare spherical PbS nanoparticles except the addition of chlorine-containing solvents such as 1,2-dichloroethane (DCE) to the oleic acid. In the absence of a DCE solvent, PbS nanoparticles were prepared as illustrated in path A of Fig. 7A. The chlorine-containing solvent modified the nucleation and growth rate during primary nanocrystal formation, which enabled survival of the highly reactive {110} surfaces in small nanocrystals during the early stage of the reaction. These tiny nanocrystals merged into 2-D nanosheets (paths B and C in Fig. 7A) because the oleic acid self-assembled monolayer exclusively decreased the surface energy of the {100} facet. Growth of the nanosheet was monitored by UV-visible spectroscopy (Fig. 7B) and HR-TEM (Fig. 7C–F). During the early stage of the reaction, small and isolated quantum dots appeared in ~50 s, as shown by the black spectrum in Fig. 7B and the HR-TEM image in Fig. 7C. As the reaction evolved, the fluorescence band of the quantum dots decreased and an absorption peak corresponding to the nanosheet became visible as the oriented attachment of the primary nanocrystals proceeded.

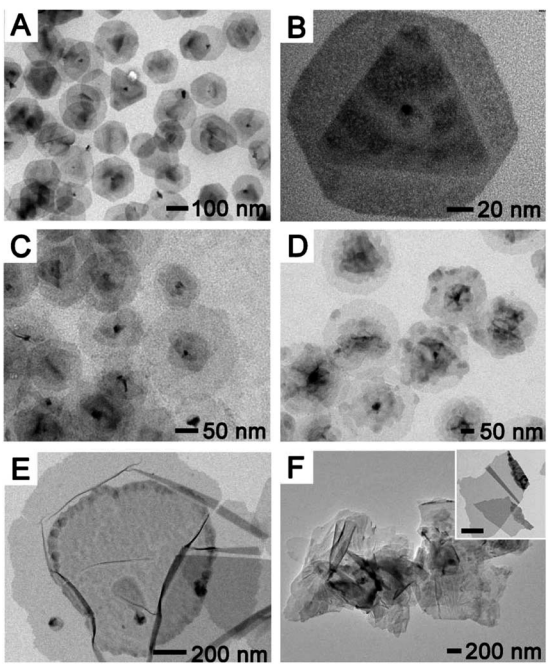

Fig. 6 TEM images showing morphological changes of the Bi_2Se_3 nanostructured materials from nanodiscs to nanosheets by controlling the molar ratio of PVP in the mixture with PEI. PVP : PEI = 10 : 0 (A and B), 9 : 1 (C), 8 : 2 (D), 3 : 7 (E), and 0 : 10 (F). The inset in F indicates the nanosheet fragments torn off from a wide sheet by applying ultrasonic sound in the suspension (scale bar = 200 nm).[136] Adapted from ref. 136 with permission from American Chemical Society.

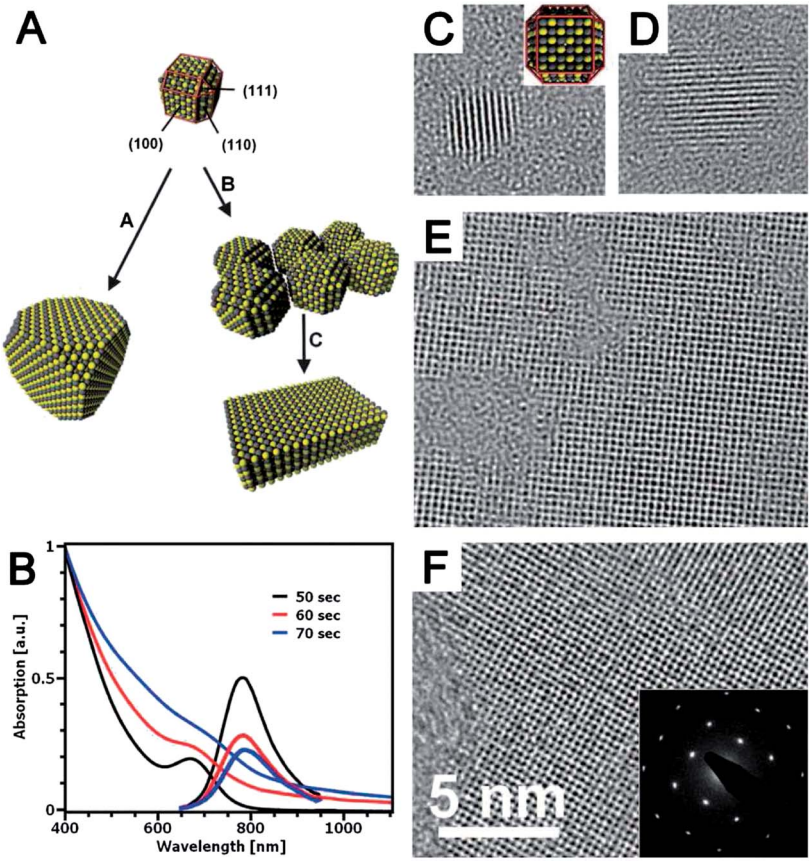

Fig. 7 (A) Schematic illustrating the two growth pathways of quasi-single PbS nanocrystals to a large particle (path A) and to a nanosheet (path B and C). (B) Absorption and emission spectra of the PbS nanocrystals according to the reaction time. (C–F) TEM images showing the shape evolution of PbS nanocrystals into a nanosheet by an oriented attachment growth mechanism.[158] Adapted from ref. 158 with permission from American Association for the Advancement of Science.

4. Chemical transformation

Chemical transformation from a premade nanocrystal into another is a powerful route to obtain nanocrystals of diverse shapes and chemical compositions that cannot be obtained directly *via* the conventional synthetic approaches.[162,163] The synthetic parameters to control the size, shape, and composition of the product nanocrystals are mingled in classical solution-based synthesis. Such multiple control factors interrupt fine-tuning of these variables. However, chemical transformation without any separate homogeneous nucleation allows systematic control over synthetic variables. Chemical transformation of nanomaterials has been exploited as a new synthetic tool to generate 1-D and 2-D nanostructures. It allows the synthesis of materials that are not obtainable by direct synthesis. The simple structure of an initial template material can be transformed into a complicated structure.

Chemical transformation can be divided into three categories based on the underlying mechanism: alloy formation, ion exchange reaction, and galvanic replacement. Alloy formation is accomplished by mutual diffusion between atoms in premade solids and dissolved atoms in a reduced form. This strategy has been used to generate various MC nanostructures with diverse morphologies including nanoparticles (ZnS,[164] CdS,[165] PbS[166]), nanotubes (Ag_2Se,[167] Bi_2Te_3,[168,169] $CoTe_2$,[170] CoTe[171]), nanowires (Ag_2Se,[66,172] Ag_2Te,[162,173] Bi_2Te_3,[174] CdTe,[175] PbTe,[175,176] La_2Te_3 (ref. 177)), heterojunction double dumbbell Ag_2Te–Te–Ag_2Te nanowires,[178] and tri-wing Ag_2Te nanoribbons.[179] Chalcogens (Se, Te) are considered an ideal model system to prepare 1-D MCs because of their inherent tendency to grow into 1-D shapes and their high reactivity with metal precursors. For example, Yu and co-workers have utilized Te nanowires as starting materials to prepare various 1-D metal telluride nanostructures (Bi_2Te_3, CdTe, PbTe).[174,175] The reaction processes were simple. Metal cations (Bi^{3+}, Cd^{2+}, Pb^{2+}) were reduced to their neutral elements (Bi, Cd, Pb) using hydrazine hydrate as a reducing agent. The neutral elements reacted with Te nanowires to form metal telluride nanowires. An example of the CdTe system is provided below:

$$2Cd^{2+} + N_2H_4 + 4OH^- \rightarrow 2Cd + N_2 + 4H_2O \quad (2)$$

$$Cd + Te\ (nanowires) \rightarrow CdTe\ (nanowires) \quad (3)$$

Exchange of metal cations in the MC nanocrystals is a useful technique to diversify the accessible material species. Chalcogen anions, which are typically larger than metal cations, play

a vital role as a frame preserving the structure of MC materials. Metal cations are mobile within their ionic structures; hence they can be replaced by other cations under appropriate conditions. Numerous research groups have used a solution phase approach to generate a 1-D chalcogenide nanostructure *via* cation exchange reactions (CdTe,[162] ZnTe,[162] PbTe,[162] and CdSe[66,180] nanowires, PbS[181] and ZnSe[182] nanorods, and $PtTe_2$ (ref. 162) nanotubes). Jeong and co-workers systematically demonstrated the chemical transformation of Te nanowires into Ag_2Te nanowires *via* a topotactic alloying process, and then subsequently conducted cation exchange using the Ag_2Te nanowires to generate diverse MC nanowires (CdTe, ZnTe, PbTe) and $PtTe_2$ nanotubes (Fig. 8A).[162] The as-synthesized Te nanowires with a single-crystal structure (Fig. 8B) transformed spontaneously into single crystalline Ag_2Te nanowires with no drastic morphological changes (Fig. 8C). This structural preservation can be explained by topotatic lattice matching between trigonal Te and monoclinic Ag_2Te lattices, despite the large volume increase during transformation. Compared to Ag_2Te, other metal tellurides (CdTe, ZnTe, PbTe) are more soluble in polar solvents, which thermodynamically prohibits cation exchange to create other metal telluride nanowires from Ag_2Te (Fig. 8D). Cation exchange was successfully accomplished by introducing a complexation ligand, tributylphosphine (TBP), which selectively binds to silver. This example proves that careful choice of ligands can facilitate thermodynamically unfavorable exchanges by reversing the solubility order. Single crystallinity was preserved in the product metal chalcogenide nanowires due to the small volume change. In the transformation of CdTe into $PtTe_2$, cation exchange was thermodynamically favorable due to the much lower solubility of $PtTe_2$ than that of CdTe. The exchange reaction caused a large volume decrease, resulting in the production of $PtTe_2$ nanotubes (Fig. 8E and F).

This approach can be used to obtain 2-D nanocrystals with non-layered crystal structures. However, the chemical transformation of 2-D nanostructures remains largely unexplored. Cheon and coworkers reported the cation exchange reaction of layered TiS_2 nanodiscs leading to toroidal Cu_2S nanostructures (Fig. 9A).[183] They first synthesized TiS_2 nanodiscs stabilized by oleylamines (Fig. 9B–D). Addition of $CuCl_2$ to the nanodisc suspension and subsequent heating at 200 °C for 30 min yielded Cu_2S toroids (Fig. 9E–G). The resulting toroids with a hole in their center were highly symmetrical and double-convex. This transformation was driven by a regioselective edge reaction and ion diffusion through nanochannels between layers. The replacement of TiS_2 with Cu ions took place at the edge of the nanodiscs during the early reaction stages, and then subsequent ion diffusion through the interlayer in the TiS_2 nanodiscs resulted in the formation of heteroepitaxial TiS_2–Cu_2S intermediates. As the replacement reaction proceeded, double-convex toroidal Cu_2S structures were generated.

In contrast to cation exchange, anion exchange causes considerable structural changes. Thus, more energy is required to overcome the kinetic barrier than that required for cation exchange. Anion exchange has rarely been explored compared to cation exchange reactions (CdS, CdSe, CdTe nanotubes).[184,185] CdSe nanotubes with CdSe thorns on their surfaces were synthesized from $Cd(OH)_2$ nanowire bundles through an anion exchange reaction by Se.[185] $Cd(OH)_2$ nanowire bundles were

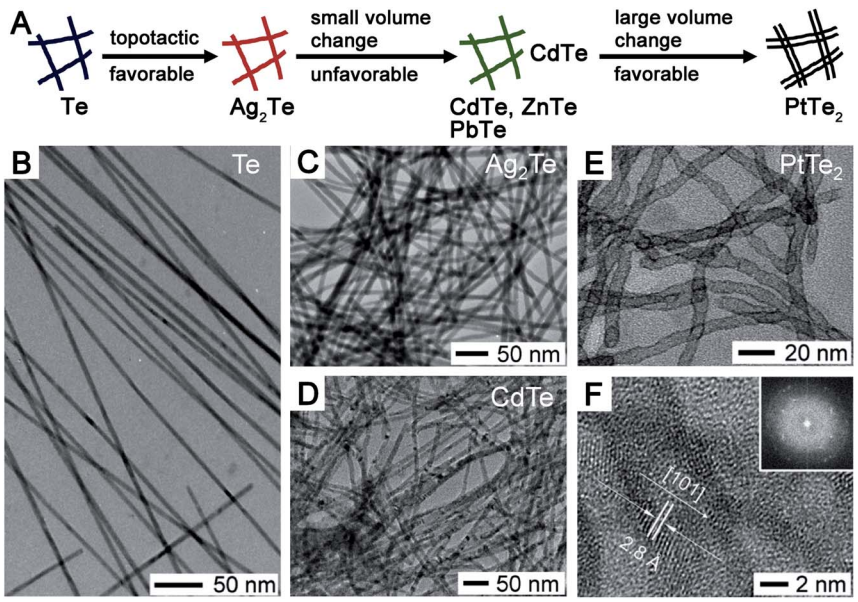

Fig. 8 (A) Flow of chemical transformation from ultrathin Te nanowires into various chalcogenide 1-D nanostructured materials. Topotactic transformation from ultrathin Te to Ag_2Te nanowires, which is thermodynamically favorable. Reversible cation exchange reaction for generating metal telluride nanowires (MTe, M = Cd, Zn, Pb) from Ag_2Te nanowires. The reaction is thermodynamically prohibited; hence the use of a specific surfactant is needed. Further transformation of CdTe nanowires into $PtTe_2$ nanotubes through a forward cation exchange reaction. TEM images of ultrathin Te (B), Ag_2Te (C), CdTe nanowires (D). TEM (E) and HR-TEM (F) images of the $PtTe_2$ nanotubes transformed from CdTe nanowires. The inset shows the Fourier transformed ring pattern of $PtTe_2$ nanotubes.[162] Adapted from ref. 162 with permission from American Chemical Society.

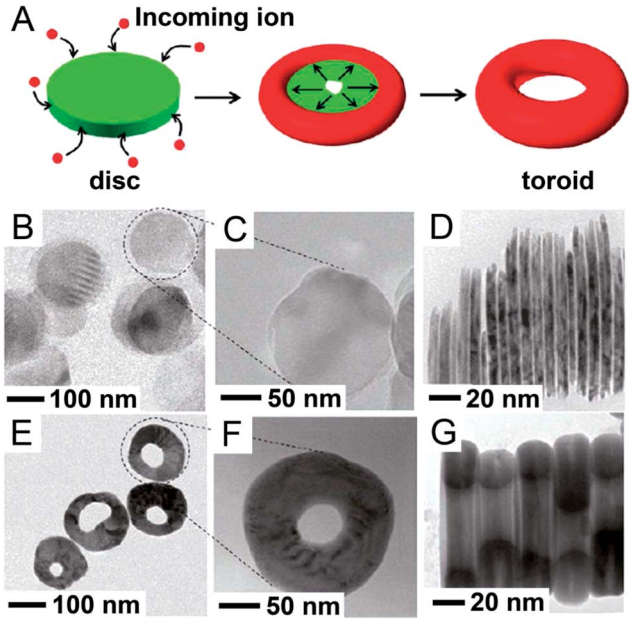

Fig. 9 (A) Schematic illustration of the transformation from a Ti_2S nanodisc into a Cu_2S toroid by regioselective reaction of Ti_2S with incoming ions. (B and C) TEM images of Ti_2S nanodiscs as a starting material. (D) Cross-sectional TEM image of a stack of Ti_2S nanodiscs. (E and F) TEM images of Cu_2S toroids transformed from Ti_2S nanodiscs. (G) Side view of a stack of Cu_2S toroids.[183] Adapted from ref. 183 with permission from American Chemical Society.

synthesized first on a glass substrate in an aqueous phase. Rapid exchange between OH^- and Se^{2-} as well as fast outward diffusion of Cd^{2+} in the aqueous solution resulted in the formation of tubular structures. Subsequent nucleation and growth of CdSe thorns on the nanotube surface proceeded until the Cd sources were consumed completely. The surface morphology of the nanotubes was dependent on the concentration of the Se ions. Nanotubes with clean and smooth surfaces were formed without any thorn at high Se concentrations, which was attributed to uniform chemical reaction along the entire length of the nanowire bundles. Meanwhile, CdSe thorns on the nanotube were generated at low Se concentrations due to localized exchange reactions with Cd^{2+} ions diffusing out from the bundles. The anion exchange reaction was also observed in tin chalcogenide structures. SnSe nanosheets with a layered structure were transformed into SnTe nanosheets with a non-layered cubic structure, *via* solution phase anion exchange.[186] The bond energy difference between trioctylphosphine (TOP) as a chalcogen complex agent and chalcogen elements drove the exchange reaction. Because the P=Se bond is stronger than the P=Te bond, TOP–Se is favorably formed in a reaction system that includes TOP–Te and SnSe, which drives the anion exchange reaction. SnTe nucleated with crystallographic alignment on SnSe nanosheets, which were consumed to yield porous SnTe nanosheets.

Galvanic replacement is considered a simple and effective way to prepare 1-D noble metal nanostructures.[187] The redox potential difference between elements leads to deposition of the more noble elements and dissolution of the less noble elements. Yang and co-workers utilized redox reactions to prepare Au, Ag, Pd, and Pt nanowires from $LiMo_3Se_3$ nanowires; the latter nanowires functioned as both templates and reducing agents.[188] Metal ions ($AuCl_4^-$, Ag^+, $PdCl_4^{2-}$, $PtCl_4^{2-}$) in aqueous solutions were reduced and subsequently deposited on the nanowire templates. Meanwhile, the nanowire templates were oxidized and dissolved in aqueous solutions. The following redox reaction between $LiMo_3Se_3$ and Au took place:

$$3LiMo_3Se_3(s) + AuCl_4^- \rightarrow Au(s) + 3Mo_3Se_3 + 3LiCl + Cl^- \quad (4)$$

Pt nanotubes, Pt nanowires, and Pd nanowires a few nanometers in diameter have been successfully prepared by galvanic replacement using Te template nanowires.[189] In a typical synthesis, metal precursors (H_2PtCl_6, $PdCl_2$) are added to an ethylene glycol suspension of Te nanowires at 50 °C. Interestingly, the resulting products had different morphologies. In the case of the Pt nanotubes, some Pt nanoshells formed during the early stages of the reaction, which permitted the inter-diffusion of reactant ions across the shell. As galvanic replacement proceeded, the Pt nanoshells grew inwards at the cost of the Te templates. Based on stoichiometric relationships, this reaction involves the replacement of equivalent molar amounts of Pt by TeO_3^{2-}. The smaller molar volume of Pt (~9 cm^3 per mol) than that of Te (~20 cm^3 per mol) yielded a tubular structure. Furthermore, the molar volume of two moles of Pd (~18 cm^3 per 2 mol) is similar to that of 1 mol of Te, which resulted in solid Pd nanowires. In 2-D nanostructures, Sb_2Te_3 hexagonal nanoplates were transformed into porous 3-D network-shaped Te plates. Tartaric acid (TA) in the reaction solution aided the dissolution of Sb^{3+} ions from Sb_2Te_3 by forming $Sb(TA)_x^{3+}$. Simultaneously, Te^{2-} ions were oxidized by O_2 to Te^0; the latter nucleated preferentially on the Sb_2Te_3 surfaces and acted as seeds for growth into porous 3-D Te plates. The Te structure was further transformed into porous Pt, Pd, and Au plates *via* galvanic replacement reactions in the presence of metal precursors (H_2PtCl_6, $PdCl_2$, $HAuCl_4$).[190]

5. Applications

Interest in anisotropic 1-D and 2-D nanostructures has been steadily increasing due to their large surface area, quantum confinement effect, and superior optoelectrical or thermoelectrical properties. Anisotropic geometry and size reduction comparable to the Debye length can alter the optical, electric, and magnetic properties of the bulk counterparts. Focusing on MCs prepared in solution phases, the major interest for practical applications is in thermoelectric power generation or electronic device cooling, high performance electrodes for batteries, nanocrystal-based photovoltaic devices, and photodetectors. Recently, new potential uses of the solution-based MC nanocrystals are being investigated, which include localized surface plasmon resonance (LSPR) and oxygen reduction reaction. MC thin films prepared by the vacuum process have shown the possibilities as a new class of materials such as topological insulators, semiconductors with a high electron mobility, and superconductors. Although the organic surfactants

indispensable in solution chemistry diminish such superior physical properties, the solution-based approach has a large scope to achieve such physical properties. This section reviews recent advances in the practical applications of the anisotropic MC nanocrystals, and introduces briefly the potential applications.

5.1. Anodes of Li ion batteries

Graphite, which is conventionally used as the anode of lithium ion batteries (LIBs), has a small theoretical capacity of 372 mA h g^{-1}, which is too low to meet the current need in electronic devices. A number of 2-D metal disulfide (MS_2) nanocrystals such as MoS_2, WS_2, and SnS_2 are considered as promising alternatives to graphite.[30–33] Their theoretical capacities are typically twice that of graphite and their layered structures (S–M–S) facilitate reversible intercalation of Li ions (Fig. 10A). The synthesis of the metal disulfides has been actively developed during the last five years. Hydrothermal and solvothermal methods have been widely used for the synthesis of the 2-D MS nanocrystals and their hybrid composite materials with graphene or CNTs.[33,191] These methods facilitate the large scale production of the high quality 2-D MS nanocrystals at low cost and in a short processing time. The thermal decomposition approach is promising to prepare the stoichiometric 2-D MS_2 nanocrystals with massive production for industrial needs.[32] Free standing 2-D MoS_2 or WS_2 nanosheets were synthesized by decomposition of single-source precursors containing metal and sulfur sources in oleylamine which could cover the surfaces of the 2-D MS nanosheets. This oleylamine molecule functions as a protective layer for the oxidation and aggregation.[192] Exfoliation of bulk materials in a liquid phase is a relatively new approach to prepare thin 2-D nanosheets.[193,194] Ultrasonic treatment in organic solvents helped the exfoliation of the bulk materials. The surface energy of the bulk material in the solvent should be minimized to lower the energy requested for exfoliation; hence the surface energy of the solvent should be similar to that of the bulk material.

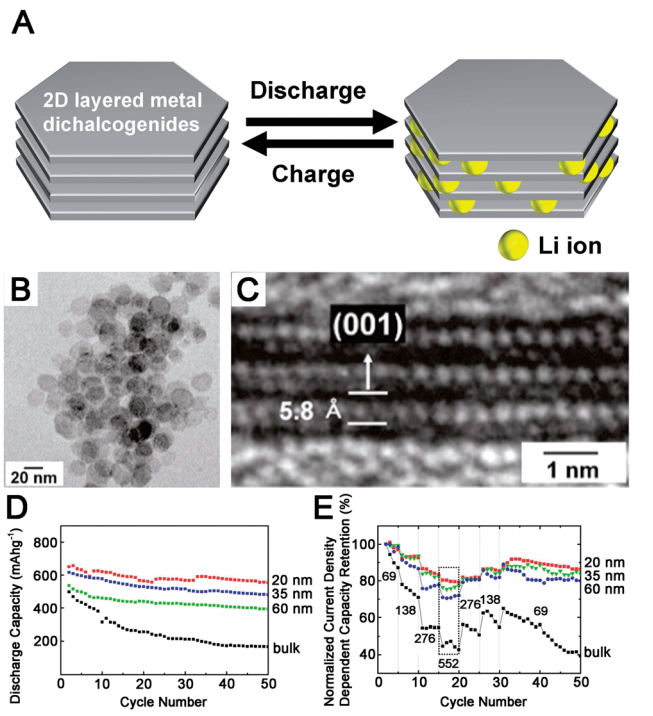

Fig. 10 (A) Schematic illustration of the reversible intercalation and exfoliation of Li^+ ions in 2-D layered anodic materials. (B) Top- and (C) side-view TEM images of as-synthesized ZrS_2 nanodiscs. (D) Cycling behaviors of ZrS_2 nanodiscs with different lateral dimensions (20, 35, and 60 nm) and bulk ZrS_2. (E) Current density-dependent capacity retention profiles of ZrS_2 nanodiscs (20, 35, and 60 nm) and bulk ZrS_2 at current densities of 69, 138, 276, and 552 mA h g^{-1}.[128] Adapted from ref. 128 with permission from American Chemical Society.

With the thermal decomposition method, Cheon and coworkers reported that LIBs with anode electrodes fabricated with 2-D SnS_2 nanoplates showed enhanced capacities.[32] The discharge capacity was as high as 1311 mA h g^{-1} in the first cycle, which is close to the sum of the theoretical irreversible capacity (587 mA h g^{-1}) and maximum theoretical reversible capacity (645 mA h g^{-1}). The average discharge capacity (583 mA h g^{-1}), close to 90% of the maximum theoretical reversible value, was stable and reversible up to 30 cycles. These excellent electrochemical properties were attributed to enhanced diffusion kinetics of lithium ions by the finite lateral size and open edges of the nanoplates. Recently, the same group synthesized ZrS_2 nanodiscs with tunable lateral dimensions (20, 35, and 60 nm) and systematically studied the effect of size on Li ion intercalation (Fig. 10B and C).[128] The average discharge capacities of the 20, 35, and 60 nm ZrS_2 nanodiscs were 586, 527, and 433 mA h g^{-1}, respectively (Fig. 10D). The 20 nm nanodiscs had a capacity 2.3 times greater than that of the bulk ZrS_2 material (255 mA h g^{-1}). The retention capacities of the small nanoplates were ~80, ~77, and ~71% of the original capacities, respectively, while the retention of bulk ZrS_2 decreased continuously and was only 39% after 50 cycles (Fig. 10E).

MS_2/carbon composite nanocrystals such as FeS/C,[154] SnS_2/graphene,[195] CoS_2/C,[196] MoS_2/graphene,[191,197] MoS_2/CNTs,[198] and MoS_2/C possess even more outstanding electrochemical properties than bare MS_2 nanoplates when they were used as anodes for LIBs.[199] Incorporation of carbon materials improves the charge current, effective surface area, and chemical tolerance of MS_2 nanocrystals. MoS_2/graphene composite nanosheets were synthesized by a one-step solution phase method.[191] The first charge and discharge capacities of the MoS_2/graphene composites were 2200 and 1300 mA h g^{-1}, respectively, which are higher than those of bare MoS_2 and graphene. In addition, the cycling behavior exhibited a reversible capacity of 1290 mA h g^{-1} for up to 50 cycles, while the reversible capacity of the bare MoS_2 electrode declined to 605 mA h g^{-1} after 50 cycles. The high capacity and enhanced cycling stability of the composite were attributed to effective and rapid charge carrier transport back and forth from the MoS_2 layers to the graphene layer. Nanostructured SnS_2, although a promising anode material for LIBs, has the drawbacks of large volume changes and accompanying decreases in capacity during electrochemical cycling.[200] One solution to minimize the volume expansion is to distribute the tin-based materials evenly

throughout another phase matrix. Zhi and co-workers prepared porous SnS_2/graphene composites through a two-step approach.[195] SnO_2 nanoparticles were formed on the surface of graphene nanosheets and then transformed into 2-D SnS_2 nanoplates by reaction with H_2S gas. The reversible capacity of the SnS_2/graphene composites was 650 mA h g^{-1} after 50 cycles, which is much higher than that of bare SnS_2 nanoplates (277 mA h g^{-1}). These results suggest that graphene layer functions both as a buffer matrix and a conducting pathway to improve cycling durability.

5.2. Photodetectors

Photodetectors that contain nanocrystal solids are some of the simplest optoelectronic devices. The electrical conductivity of the nanocrystal solids changes under illumination due to the increase in density of mobile charge carriers.[201] Photodetectors require high sensitivity, selectivity, and stability. Many MCs have high absorption coefficient and good photostability, which are excellent characteristics of photodetecting materials. Various MC nanowires have been tested for the purpose because of their tunable electronic structure and band gap as well as the enhanced conduction of charge carriers in the length direction. Among various 1-D MC nanocrystals,[202–211] silver sulfide (Ag_2S) is known as an excellent optical sensing material with a superior chemical stability. Li and co-workers reported a simple route to generate single crystalline Ag_2S nanowires that involves addition of sulfur powder into an octadecylamine solution containing a $Ag(NO)_3$ precursor at 120 °C (Fig. 11).[211] The nanowires had diameters ranging from 10 to 30 nm and lengths up to hundreds of micrometers. The photoelectric properties of the individual Ag_2S nanowires were investigated under UV illumination. The current increased sharply from 2.3 to 594 pA upon UV illumination, but the current decreased to dark current within 1 s upon turn-off of the UV light. This time-resolved photocurrent indicates that the dynamic response was stable and reproducible during the on-and-off states (Fig. 11B). Furthermore, the photocurrent increased as the pressure decreased without detectable changes in the dark current (Fig. 11C). Golberg and co-workers demonstrated a fast response photodetector made of Sb_2Se_3 nanowires synthesized by a hydrothermal process.[208] The current sharply increased from 4 pA (dark state) to 58 pA under 600 nm illumination. The rise and decay times were below 0.3 s. The rapid response time, high sensitivity of external quantum efficiency, good chemical stability, and good conduction along their length direction indicate that Sb_2Se_3 nanowires are promising candidates for photodetector devices.

Compared to conventional one-component (inorganic or organic) photodetectors, organic–inorganic hybrid photodetectors have unique features conferred by combination of the low ionization potential of organic molecules and the high electron affinity of inorganic components. These hybrid devices provide good physical flexibility and tunable functionality. Hybrid photodetectors with different combinations of organic and inorganic components have been fabricated.[212–214] Hybrid photodetectors composed of conjugated polymer, poly(3-hexylthiophene) (P3HT), and CdSe nanowires were fabricated on a rigid SiO/Si substrate, a flexible PET substrate, and printing paper.[215] These devices showed an enhanced photocurrent and more rapid response and recovery times than photodetectors fabricated using only one component. This was attributed to the high hole-transport rate of the polymer P3HT, the high electrical conductivity of the CdSe nanowires, and the synergistic effect of absorption spectra in the visible range. The devices fabricated on flexible substrates exhibited good flexibility, folding strength, excellent wavelength-dependent electrical stability, and rapid response to high-frequency light signals.

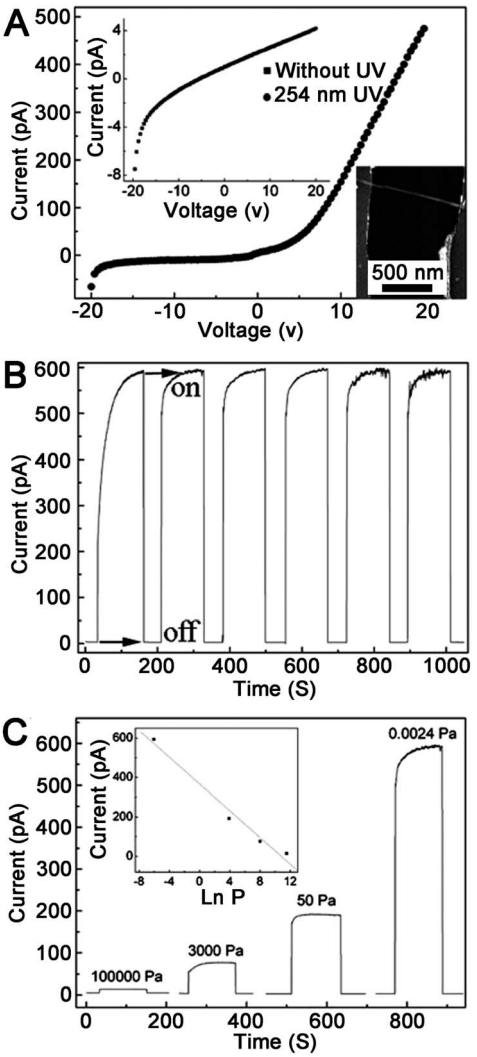

Fig. 11 (A) *I–V* characteristics of an individual single-crystalline Ag_2S nanowire under dark (top-left inset) and UV illumination at 254 nm. The measurement was done at room temperature and a pressure of 2.4×10^{-3} Pa. Bottom-right inset shows a typical SEM image of the device. (B) Time-resolved photocurrents of the device measured at a pressure of 2.4×10^{-3} Pa in air at atmospheric pressure. (C) Time-resolved photocurrents measured at different pressures. Linear relationships between the logarithmic pressure and the current (inset in panel C).[211] Adapted from ref. 211 with permission from Wiley VCH.

5.3. Thermoelectric devices

Solid-state power generation and cooling systems based on thermoelectric effects have received great attention.[26,216–218]

Thermoelectric devices composed of p- and n-type semiconductors can directly convert waste heat to electricity and *vice versa*. Bi_2Te_3 and Bi_2Te_3-based materials containing elemental Se or Sb are some of the best thermoelectric materials at low temperatures (~80 °C) and PbTe-related materials are also strong candidates at slightly higher temperatures (~300 °C). Therefore, they have been widely used in low temperature power generation and small-scale cooling of electronic devices. The energy conversion efficiency of a thermoelectric device is evaluated by the dimensionless thermoelectric figure of merit (ZT), $ZT = S^2\sigma T/\kappa$, where S, σ, T, and κ are the Seebeck coefficient, electrical conductivity, temperature, and thermal conductivity, respectively. Recent theoretical and experimental advances have confirmed that introduction of nanoscale constituents increases the power factor ($S^2\sigma$) through a quantum confinement effect. The nano-sized grains reduce thermal conductivity (κ) more effectively than the reduction in electrical conductivity (σ). Furthermore, introduction of heterostructures in the nanocomposite can increase the Seebeck coefficient (S) due to a carrier filtering effect.[137,218–220] In this respect, better control over the grain size and shape of thermoelectric nanocrystals can be obtained using a bottom-up solution approach.[221–227]

Wu and coworkers synthesized 1-D barbell-shaped Bi_2Te_3–Te–Bi_2Te_3 heterostructures consisting of a Te nanowire and Bi_2Te_3 plates set at the two ends of the nanowire (Fig. 12A and B).[227] They used a two-step conversion process. Te nanowires were synthesized by reducing tellurium dioxide with a hydrazine hydrate solution. Once the formation of Te nanowires was completed, a bismuth nitrate solution was hot-injected into the Te nanowire suspension at 160 °C, which allowed the Te nanowires to be converted into the barbell-shaped Te–Bi_2Te_3 heterostructures. By keeping the concentration of Bi low, Bi deposited onto the axial growth tips and suppressed the random deposition on the surfaces in the radial direction. The heterostructured composite was fabricated by hot pressing. ZT of the heterostructured composite was two orders higher than that of a pure Te nanowire composite (Fig. 12B). The improved thermoelectric properties are mainly due to the enhanced Seebeck coefficient (S) caused by the carrier filtering and the decreased thermal conductivity (κ) caused by phonon scattering.

In terms of the grain boundaries to enhance the phonon scattering, thin 2-D nanostructures such as nanoplates or nanosheets are promising because their face-to-face packing can generate tremendous boundaries along the pathway of the phonons. Several groups have investigated 2-D Bi_2Te_3-related structures in the past decade.[137,221–224] Hyeon and coworkers synthesized Bi_2Te_3 nanoplates with a thickness of ~1 nm. They investigated the thermoelectric properties of bulk pellets prepared by spark plasma sintering (Fig. 12C and D).[223] Both the electrical (σ) and thermal (κ) conductivities increased as the sintering temperature was raised due to enhanced densification and grain growth during sintering. A maximum ZT value of 0.62 was achieved at 400 K from the nanoplate bulk pellets sintered at 250 °C (Fig. 12D).

Challenging issues associated with the use of nanocrystals in electric devices are removal of organic surfactant and thermal

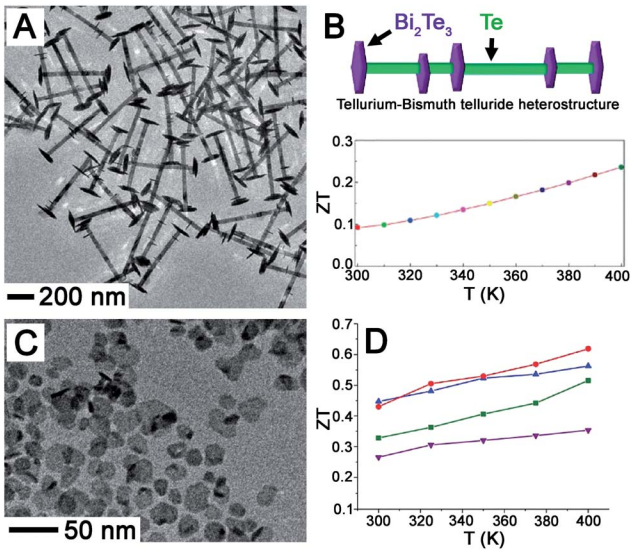

Fig. 12 Thermoelectric application of the Te–Bi_2Te_3 1-D heterostructure and Bi_2Te_3 2-D nanoplate. (A) TEM image of a Te–Bi_2Te_3 heterostructure. (B) Schematic drawing of the Te–Bi_2Te_3 heterostructure and temperature dependence of the thermoelectric figure of merit (ZT) of the sintered bulk nanocomposite pellet. Reproduced with permission.[227] (C) TEM image of the as-synthesized Bi_2Te_3 nanoplates. (D) Temperature dependence of the thermoelectric figure of merit of the Bi_2Te_3 nanoplate bulk pellets. The colors indicate the sintering temperature: 200 °C (green squares), 250 °C (red circles), 300 °C (blue upwards-pointing triangles), and 325 °C (purple downwards-pointing triangles).[223] Adapted from ref. 227 and 223 with permission from American Chemical Society.

treatment without severely damaging the as-synthesized materials. A high sintering temperature (typically >400 °C) is required to decompose the organic surfactants. The insulating organic residue left behind by incomplete removal caused the material density of the pellet to be low and decreased the power factor of thermoelectric devices. Specifically, MC nanocrystals can form multi-component alloys at high sintering temperatures, which is not desirable for high-performance, reliable devices. Jeong and coworkers demonstrated scalable, high-yield production of surfactant-free Bi_2Te_3 and Bi_2Se_3 nanoflakes.[137] Simple mixing of the nanoflake suspensions allowed homogeneous distribution of the two nanocrystal species; hence fine control of the chemical composition of the Bi_2Te_3/Bi_2Se_3 nanocomposites was possible. The ZT value was 0.7 at 400 K for a broad range of Bi_2Se_3 contents (10–15 wt%), which is highly advantageous in preparing reliable devices because the ZT value of three component alloy nanocrystals ($Bi_2Te_{3-x}Se_x$) is too sensitive to the atomic composition of Se (x).

5.4. Solar cells

MC semiconductors have been considered promising materials for the absorber layer and charge transport layer in thin film photovoltaic devices such as CdTe solar cells and CI(G)Se solar cells. The chalcogenide films in the cells with a high power conversion efficiency (η) have been prepared by chemical bath deposition (CBD) or vapor phase deposition including

evaporation, sputtering, sublimation, vapor transient deposition (VTD), and chemical vapor deposition (CVD).[228–230] Recent advances in colloidal science have facilitated simple and eco-friendly synthetic approaches to produce various nanocrystals for use in photovoltaic devices. Use of the nanocrystal inks can significantly reduce production costs through the inexpensive deposition methods such as spraying, doctor blading, spin-casting, dip coating, and roll-to-roll printing. Although the films prepared from the MC nanocrystals have been considered inferior to the conventional films made by the vacuum processes, the solution-processed thin film solar cells have undergone continuous improvement in the conversion efficiency.

Several research groups have devoted considerable effort toward synthesizing various colloidal nanocrystal inks.[40–43,231,232] In contrast to quasi-spherical nanocrystals, 1-D nanostructures may enhance carrier mobility and device efficiency by reducing the frequency of electron hopping and electron–hole recombination in the absorber layer film.[11,233,234] Korgel and co-workers demonstrated a photovoltaic device made of $CuInSe_2$ nanowires.[234] The nanowires were 20 nm thick and several micrometers long. These were indium-deficient with an average composition of $Cu_{1.0}In_{0.6}Se_{2.0}$. A free-standing fabric made of the nanowires was used to measure the photovoltaic response. Although the efficiency of the device was low ($\eta = 0.1\%$) due to the low open circuit voltage (V_{oc}) and fill factor (FF), these results exhibited the feasibility of $CuInSe_2$ nanowires as the active layer for photovoltaic devices. The low power conversion efficiency originated from the voids and the random orientation of the nanowires, which reduced conductivity and prevented the carrier transport to their corresponding electrodes. The nanowire/quantum dot composite device enhanced transport connectivity. Conversion efficiency could potentially be improved by preparing defect-free nanowires and optimizing the alignment of the nanowires. Combining nanowires with spherical nanocrystals could also potentially improve device performance. Incorporating colloidal CdSe quantum dots into CdSe nanowires improved the conversion efficiency ($\eta = 0.13\%$) and photovoltaic performance.[233] A photovoltaic device comprising CdSe quantum dots and CdTe nanorods as the active layer has also been reported.[235] Due to the band alignment between the CdSe and CdTe nanocrystals, excited electrons transferred to the CdSe phase, while holes moved to the CdTe phase. Sintering of the nanorods enhanced the carrier mobility and the power conversion efficiency ($\eta = 2.9\%$). Lin and coworkers utilized wurtzite-structured CdSe nanowires to fabricate a solar cell with the configuration of ITO/ZnO/CdSe NWs/PEDOT:PSS/Pt. They reported a conversion efficiency of 3.6% for this configuration.[236]

A remarkable improvement of the power conversion efficiency has been achieved in the solar cells based on the I–III–VI_2 nanocrystals such as $CuInSe_2$ (CISe) and $Cu(In_xGa_{1-x})Se_2$ (CIGSe).[237–239] Facile solution synthesis of CISe and related nanocrystal inks has been developed to prepare nanocrystal inks. In addition to 0-D nanocrystals,[40–43] anisotropic 1-D and 2-D crystals in the forms of $CuInSe_2$ nanowires,[240] $CuInSe_2$ nanoplatelets,[241] $Cu_{2-x}S_ySe_{1-y}$ nanowires,[242] $CuIn_{1-x}Ga_xS_2$ (CIGS) nanorods,[243] and Cu_2ZnSnS_4 (CZTS) nanorods[244] have been synthesized by the solvothermal method in the presence of the corresponding organometal precursors. Fine control of the chemical composition of the nanocrystals is the pre-requisite for a high performance device. Grain growth of the nanocrystals into high quality large crystals without incorporation of micropores is another key factor. Agrawal and coworkers reported 5.5% efficiency using the CISe nanocrystal absorber layer after solid state densification of the layer during the selenization process.[238] Very recently, the same group prepared a CIGS absorber layer film and partially exchanged the S anions with Se to form a CIGSSe layer. They reported 12% conversion efficiency by the process.[237] Jeong *et al.* achieved 8.2% efficiency with a CISe nanocrystal layer followed by high temperature densification.[239] In spite of the abrupt increase of the conversion efficiency, the chemical composition of ternary or quaternary MCs has yet to be controlled. And the effect of the nanocrystal shape has not been studied. Regarding the densification of the nanocrystal layer, *in situ* self-assembly of the 1-D or 2-D nanocrystals into superstructures during the coating process may facilitate the formation of a non-porous crystal layer. The organic surfactants obstruct densification of the nanocrystals and the vapors cause elemental contamination which is not controlled. The synthesis of surfactant-free multi-component nanocrystals is in great requirement.[245]

Conjugated polymer–MC bulk heterojunction hybrid solar cells have been actively prepared during the last ten years.[246–248] These hybrid systems take advantage of the flexible nature of polymers and the wider light absorption of inorganic materials than organic materials. Most polymer-based hybrid solar cells consist of an interpenetrated network of electron donor and acceptor phases with bulk heterojunction interfaces. Alivisatos and co-workers first demonstrated a CdSe nanorod/poly-(3-hexylthiophene) (P3HT) hybrid solar cell created by spin casting a solution of CdSe nanorods in P3HT.[249] Because CdSe and P3HT exhibit complementary absorption spectra in the visible spectrum, devices composed of blended nanorod–polymer materials have a wide photocurrent spectrum from UV to 720 nm. A power conversion efficiency of 1.7% was obtained. Since then, conversion efficiency has been steadily increased by adding additives to enhance the crystallinity of P3HT[250] or using different conjugated polymers.[251,252] Conjugated polymers used widely in hybrid solar cells have relatively large band gaps (~1.9 eV), which limit absorption of the low energy solar spectrum from red to NIR. Low band gap polymers are promising candidates as organic components for efficient light harvesting. Recently, CdSe tetrapods were combined with a low bandgap polymer (PCPDTBT), resulting in a power conversion efficiency of 3.13% under AM 1.5 illumination (Fig. 13).[253] MC nanocrystals have also been used as light-absorbing sensitizers in organic–TiO_2 heterojunction hybrid solar cells. Although the performance of these solid-state DSSCs is lower than that of liquid-electrolyte-based DSSCs, the recent progress reported by Gratzel and coworkers is promising. This group generated Sb_2S_3 nanoparticles on a porous TiO_2 layer by chemical bath deposition, and then the pores were filled with P3HT by spin-coating.[254] The resultant hybrid cell showed a high conversion

efficiency (η = 5.13%) and highly stable photovoltaic performance in air without sealing the cell. Seok and coworkers further investigated the same system to find the best conducting polymer for hole injection from the Sb_2S_3 sensitizer nanocrystals. They achieved η = 6.18% at 1.5 AM 1.5 G radiation.[255] So far, spherical quantum dot sensitizers have been used attached to the surfaces of the porous metal oxide network. Anisotropic MCs such as nanorods and nanoplates deserve thorough investigation for the hole injection and chemical correlation with the polymer layer.

5.5. Other potential applications

Besides the aforementioned applications, the solution-based MC nanocrystals have recently been investigated as potential materials for localized surface plasmon resonance (LSPR) and oxygen reduction. The topological insulating property and superconductivity of layer-structured MCs are now actively considered in physical studies. Although most current studies have been conducted with MCs prepared through the vacuum processes, a solution-based approach is still advantageous in producing copious amounts and in structural control.

Surface plasmon is a light wave that evolves as a result of resonant interactions between the electromagnetic field of incident light and the plasma of electrons confined in restricted dimensions. Plasmons confined in nano-sized dimensions oscillate locally with a frequency known as the localized surface plasmon resonance (LSPR). The intensity and frequency of surface plasmon absorption bands are highly dependent on the characteristics of the material, such as the material species, size, shape, and additives on the surface.[256] Resonant waves are sensitive to the dielectric properties of the surrounding and can be tuned by external electromagnetic waves,[257] which enables the surface plasmon to be utilized for sensing,[258] imaging,[259] information processing,[260] and optoelectronic purposes.[261] LSPRs have been extensively characterized with metal nanoparticles (Au, Ag, Pt, Cu *etc.*). Semiconductors have an additional control variable in LSPR, which is tunability of the carrier concentration by doping. Copper chalcogenide nanocrystals are the species studied the most so far.[262–265] When Cu is slightly deficient with respect to S or Se, the nanocrystals contain a large number of free hole carriers in the valence band. The LSPR bands of CuS nanoparticles blue-shifted as the dopant concentration was increased. Recently, the effects of morphology on the LSPR response has been investigated in a $Cu_{2-x}S$ nanodisk system.[37] In-plane and out-of-plane dipolar resonances were determined. The wavelengths, line shapes, and relative intensities of these plasmon bands were tuned by controlling the geometric aspect ratio of the disk or free carrier densities.

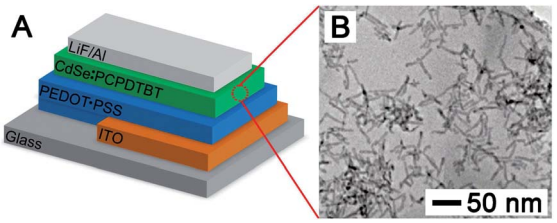

Fig. 13 (A) Photovoltaic device configuration of a CdSe–PCPDTBT hybrid structure. (B) TEM image of CdSe tetrapod nanocrystals as the component of active layers.[253] Adapted from ref. 253 with permission from American Chemical Society.

Most research on the cathodes of fuel cells has focused on Pt-based materials because of their excellent electrocatalytic performance. However, Pt-based materials show severe Pt-dependence,[266] the kinetics of the oxygen reduction reaction (ORR) are slow,[267] and there is CO deactivation.[268] Various MCs are considered promising Pt-free ORR electrocatalysts because of their low cost, high tolerance to methanol and halide ions, and simple solution-based synthetic approach.[269] For example, $CoSe_2$–DETA (DETA = diethylenetriamine) hybrid nanobelts show good electrocatalytic performance with respect to ORR (onset potential of *ca.* 0.71 V) in acidic media. This good performance is ascribed to the large specific surface area and well-defined layered structure of $CoSe_2$–DETA constructed with small DETA molecules.[270] Long-term stability of the $CoSe_2$–DETA still needs to be addressed before these can be used practically.[270] The properties of MC cathodes can be improved by introducing other nanoparticles. For example, adding Fe_3O_4 nanoparticles to the $CoSe_2$ hybrid nanobelt catalyst resulted in an increase of onset potential and current density.[270] Although the electrocatalytic activity of this catalyst is still lower than that of Pt-based catalysts, these hybrid MC systems deserve further investigation.

A topological insulator is an unconventional quantum phase of semiconducting or insulating matter that possesses a metallic conductivity on its surface.[271–273] Surface electronic states are spin polarized and protected by time-reversal symmetry. Significant efforts have been devoted to investigate the potential application of topological insulators in spintronics and quantum information processing.[274,275] The number of publications on the layered MC materials, mainly V–VI (V = Bi, Sb; VI = Se, Te), has been increasing dramatically since this family of compounds was predicted to be three-dimensional topological insulators with unique surface states composed of a single Dirac cone at the Γ point.[276–279] Currently, most studies on topological insulators have been conducted with chalcogenides obtained through vapor-phase synthesis. Fine control of the thickness, defects, and atomic states at the surfaces are challenging issues. And the synthesis of wide 2-D MC nanosheets (larger than at least a few micrometers) should be synthesized in a highly reproducible manner. And, the organic surfactants are serious obstacles to the solution-based MC nanocrystals in this area. Surfactant-free or inorganic surfactant systems during the preparation of MC nanocrystals create the clean surface and cause the negligible change of the surface electronic state. Solving these issues of synthesis is expected to draw attention in MC-based transistors.

Some MCs have recently emerged as a new class of superconductors that are electrically conductive without resistance below a certain temperature.[280–282] Iron chalcogenides (FeSe, FeTe) with a layered structure are considered high-superconducting transition temperature (T_c) superconductors.[283] In

addition, unconventional superconducting states are expected from the interaction between magnetism and superconductivity. Iron selenide (FeSe) has shown superconducting properties with a T_c of 8 K.[284] The T_c of FeSe is improved up to ~14 K by doping Te[285] and to over 30 K under high pressure with a dT_c/dP rate of ~9.1 K Gpa^{-1}.[286] Sulfur-doped $FeSe_{1-x}S_x$ systems (x = 0.2) have a T_c of 15.5 K.[287] Superconductivity above 30 K was recently reported for $K_{0.8}Fe_2Se_2$ due to alkali intercalation between the FeSe layers.[288] Despite recent advances in iron-based superconductors, their chemical complexity, local structure, and the relationship between magnetism and superconductivity need to be understood to clarify the mechanism.[289] Unfortunately, no MCs synthesized by a solution approach have been reported to possess superconductivity. We attribute this to the difficulty in fine control of the chemical composition, defects, and surface states in solution-based approaches. It is a challenging subject to realize the superconductivity in the materials synthesized in a solution.

6. Challenges

This review summarized four different approaches to synthesize anisotropic MC nanocrystals: intrinsic growth into a 1-D or 2-D nanostructure, crystal growth in organic templates, oriented attachment, and chemical transformation. A number of challenges should be addressed in the solution-based synthesis of the anisotropic MC nanocrystals to realize practical applications in industry. The challenges include (1) understanding of the surface energy decrease by surfactants, (2) adopting chemical transformations in the nucleation and growth of MC nanocrystals, (3) removal of organic surfactants, (4) kinetic study on the chemical transformation, (5) scale-up of production to meet the industrial needs, and (6) eco-friendly synthesis.

In the synthesis utilizing organic surfactants, the decrease in surface energy depends on the number of binding sites and the binding energy between the surfactant molecules and the inorganic surfaces. Binding exclusively to a specific surface can facilitate the oriented attachment to form nanowires or nanoplates, but binding to all the surfaces helps self-assembly of the nanocrystals into superstructures. In the layer-structured materials, the number of crystal surfaces exposed to the solution is limited (typically 2 surfaces) and the surfactant molecules adsorb on the top and bottom surfaces without binding to the side surface. The small flat nanocrystals go through the oriented attachment side-by-side and form larger nanoplates or nanosheets; hence oriented attachment in 2-D structures is natural as seen in many recent publications.[136,158,161] In contrast, the oriented attachment for generating 1-D nanomaterials requests delicate control of binding of surfactant molecules. The small building block nanocrystals to be used for this oriented attachment may be isotropic or show small deviation from an isotropic shape. The number of surfaces of those nanocrystals is large and the atomic composition of the surfaces is not simple. To succeed in exclusive binding of surfactant molecules to a specific surface of the building block nanocrystals, we need precise quantitative information on the binding energy and the resulting surface energy decrease. Unfortunately, the information is yet to be understood because the binding is affected by as many reaction conditions as surfactant molecules, MC crystal structures, precursors, solvents, temperature, pH, *etc.* An additional issue regarding the surfactant is the assembly of the building block nanocrystals that are driven by interactions between the surfactant molecules. These surfactant interactions may induce self-assembly of the building blocks to form superstructures or cause the formation of templates such as micelles or vesicles consisting of the surfactant molecules and the MC elements. Currently, it is not clear which molecules can exist as the organometal complex and form such templates during the synthesis. Several anisotropic MCs have been prepared by the template-based synthesis, but the physics on the formation of such templates needs thorough investigation. The physics is more complicated than the micelle formation of pure organic molecules because the interaction between the inorganic elements incorporated in the organic molecules should be taken into consideration in the assembly of the complex molecules.

Another challenge in the synthesis of anisotropic MC nanocrystals is the lack of knowledge on how the chemical composition of the nanocrystals is determined. The theory of conventional nucleation and growth in a solution phase has been established under the assumption of stoichiometric supply of elemental sources. The concentration of a source element is determined by the reduction rate of the precursor. Finding synthesis conditions under which the reduction rates of the source molecules are the same is critical in the nanocrystal synthesis. It is not certain whether the elemental composition of a product nanocrystal is identical to the elemental concentration of the sources in the nucleation and growth steps. Because the equilibrium constants of the precursors are different and vary during the synthesis, it is almost impossible to maintain the stoichiometric concentration of the source elements. This hypothesis leads to the existence of chemical transformation taking place during the nanocrystal synthesis. In the MC nanocrystals, the *in situ* chemical transformation is the alloy formation.[163] Taking an example of CdSe quantum dots, the nuclei might be Cd-rich or Se-rich or even pure Cd or Se, and then the other element forms alloy nanocrystals with the stoichiometric composition of 1 : 1. The alloy formation is spontaneous because the alloy composition is thermodynamically more stable. As long as initial nuclei do not grow into an anisotropic structure, the overall shape of the final product will be 0-D and the precise facets will be determined by surface energy of the nanocrystal. Hence, the shape of 0-D nanocrystals is not very sensitive to reaction temperature. In the anisotropic MC nanocrystals, however, the fast anisotropic growth of one component can result in a completely different shape of the final product although the chemical compositions of the nanocrystals are identical. For example, The shape of Bi_2Te_3 is strongly dependent on the reaction temperature, typically varying from 2-D nanoplates at high temperatures (~200 °C) to nanowires with lots of nanoplates growing in the radial direction at lower temperatures (~150 °C), or to nanowires with multiple grains at much lower

temperatures (~100 °C).[290] At the high temperatures, the elemental fraction of the reduced Bi and Te is considered similar to 2 : 3; hence the stable stoichiometric 2-D nanoplates could be nucleated and grown. At the low temperatures, Te grows first into the nanorods or nanowires because of its intrinsic preference to a 1-D structure, and then they are transformed into Bi_2Te_3. The shape of the final product should depend on the length of pure Te nanowires before Bi starts forming the alloy. This result is an example showing the importance of understanding the reaction kinetics in the shape control of anisotropic nanocrystals. Unfortunately, the kinetics has not been studied thoroughly. For the ternary or quaternary nanocrystals, monitoring the reaction kinetics is a very difficult task at the current stage. Data on the basis of the reduction rate of the precursors under a variety of solution conditions should be accumulated by both experimental and theoretical studies.

Surfactants are critical in preparation of stable colloidal suspensions and in the shape control of MC nanocrystals. However, the organic surfactants are problematic in practical uses. Many applications involve sintering of the MC nanocrystal films which aims at preparation of nanograined composites (thermoelectric devices) or simply at solution processing for cost-effective device fabrication (CI(G)S solar cell). The insulating organic layer functions as a barrier for charge injection and diminishes the expected properties from the pure MCs. The surfactant molecules change the surface electronic state of the individual MC nanocrystals; hence studies on the topological insulator and the high-mobility semiconductor have been conducted with the MC films obtained by the dry-processes. Nanocrystal thick films often exhibit weak mechanical strength caused by the low material density and micropores generated during the sintering of the nanocrystal films. The problem regarding the use of surfactants can be tackled by the synthesis of surfactant-free nanocrystals, ligand exchange by volatile organic molecules, or the use of inorganic surfactants. The surfactant-free synthesis is promising for the 2-D MC nanocrystals because their basal surfaces are covered with chalcogen atoms. The slightly negative charge of the chalcogen atoms can provide colloidal stability to the nanocrystals. Although the stability without a surfactant is limited, the nanoplates can be redispersed in the solution by simple ultrasonication and formulated into nanocrystal inks. If the application is to produce thick films of MC crystals through thermal treatment, a slurry-like ink is useful for the coating process. When the long-term stability is critical, the organic surfactant can be replaced by volatile molecules before being used. Employing inorganic ligands appears promising because such surfactants do not form the insulating barrier layer on the nanocrystal surfaces. The approach allows low-temperature thermal annealing which facilitates fabrication of flexible devices on polymer substrates. Furthermore, the inorganic surfactants are expected to maintain the high charge mobility and topological insulating nature of the 2-D MC nanocrystals. Recently, molecular metal chalcogenide complexes (MCCs) based on a Sn or Cu metal element have been successfully employed as the inorganic surfactants.[144,145] The other MCCs should be developed for diverse MC compositions.

The nanocrystals can be used as templates that can be chemically transformed into diverse anisotropic nanocrystals. However, thermodynamic aspects and the reaction kinetics of the chemical transformation are not well established yet. Solubility products of the reactant and the product MC nanocrystals are considered to determine whether the reaction can proceed or not. When the product nanocrystal has a lower solubility in the solution than that of the reactant nanocrystal, the reaction takes place spontaneously. Otherwise, the chemical transformation requests addition of organic molecules which bind selectively to one element of the initial nanocrystal so that the solubility product of the initial nanocrystal can be increased. So far, the solubility products of MC materials are rarely obtainable under most solution conditions. And, the binding energy between organic molecules and inorganic elements has not been tabulated thoroughly; hence selective bindings to adjust the solubility are not available in the database. The chemical transformation involves material diffusion, rearrangement of crystal structure, and accumulation of mechanical stress. The reaction kinetics and mechanism to preserve the single crystallinity during the transformation should be explored further to study the crystal structure of the product nanocrystals.

Precise shape control and heterostructure design are the main advantages of the solution-based synthesis. When it comes to the amount of production, mechanical milling of bulk MCs into a fine powder is more profitable in terms of cost. Because most applications of the anisotropic MC nanocrystals use thick films sintered at high temperatures, the gram scale production is not sufficient. For example, one pellet specimen for thermoelectric test requests about 0.5 g of nanocrystals. The CIGS solar module or a set of LIB coin cell electrodes also need similar amount for each test. Recently, a few groups demonstrated a high yield synthesis in the scale of about 1.4 g per 180 ml.[137] The synthesis should be scaled up to kg production per batch for industrial use. Obstacles to achieve the massive production are the relatively low solubility of the MC precursors, pressure build-up by the gaseous by-products during the synthesis, and inhomogeneous mixing in large scale reactors which is problematic in fast reaction systems. Continuous-flow reaction systems can be an alternative way to the batch systems. Fast mixing, easy temperature control, and small amount consumption of reagents are advantageous over the batch-type reaction. Recently, Seeberger and coworkers demonstrated a microfluidic system to produce isotropic quantum dots.[291] Jeon and coworkers reported the synthesis of ZnSe@ZnS core–shell quantum dots in a microfluidic reaction system.[292] Production of anisotropic nanomaterials has not been reported in the continuous reaction systems. Scale-up of the continuous-flow reaction and the parallel integration of the set-up may facilitate massive production to meet the industrial needs.

Nanocrystal inks are gaining tremendous attention to achieve a cost-effective coating process. Eco-friendly synthesis becomes important. Currently, MC nanocrystals are synthesized mainly by the solvothermal approach in which the reaction is conducted at a high temperature (typically around 200 °C) in organic solvents. The use of solvents with a high boiling

temperature in the approach makes it difficult to recycle the solvents. Synthesis in water or volatile alcohols is desirable in terms of the environment friendliness. The reaction yield of 100% is also an important issue in the inorganic synthesis in order to prevent contamination by toxic elements. Especially the chemical transformation approach uses an excess amount of a source material for the exchange reaction when the transformation is not favored in energetically.[162]

Acknowledgements

This work was supported by Samsung Research Funding Center of Samsung Electronics under Project Number SRFC-MA1301-07 and the Global Frontier R&D Program (2013-073298) on Center for Hybrid Interface Materials (HIM) funded by the Ministry of Science, ICT & Future Planning. Computational resource has been provided by the KISTI supercomputing center (KSC-2013-C3-040).

References

1 W. Shi, R. W. Hughes, S. J. Denholme and D. H. Gregory, *CrystEngComm*, 2010, **12**, 641.
2 C. Burda, X. Chen, R. Narayanan and M. A. El-Sayed, *Chem. Rev.*, 2005, **105**, 1025.
3 P. R. Sajanlal, T. S. Sreeprasad, A. K. Samal and T. Pradeep, *Nano Rev.*, 2011, **2**, 5883.
4 J. Zhu, B. S. Shim, M. D. Prima and N. A. Kotov, *J. Am. Chem. Soc.*, 2011, **133**, 7450.
5 D. Azulai, T. Belenkova, H. Gilon, Z. Barkay and G. Markovich, *Nano Lett.*, 2009, **9**, 4246.
6 J.-Y. Lee, S. T. Connor, Y. Cui and P. Peumans, *Nano Lett.*, 2008, **8**, 689.
7 S. De, P. E. Lyons, S. Sorel, E. M. Doherty, P. J. King, W. J. Blau, P. N. Nirmalraj, J. J. Boland, V. Scardaci, J. Joimel and J. N. Coleman, *ACS Nano*, 2009, **3**, 714.
8 A. S. Arico, P. Bruce, B. Scrosati, J.-M. Tarascon and W. V. Schalkwijk, *Nat. Mater.*, 2005, **4**, 366.
9 H. Li, Z. Wang, L. Chen and X. Huang, *Adv. Mater.*, 2009, **21**, 4593.
10 X. Wang, L. Zhi and K. Mullen, *Nano Lett.*, 2008, **8**, 323.
11 A. I. Hochbaum and P. Yang, *Chem. Rev.*, 2010, **110**, 527.
12 B. M. Kayes, H. A. Atwater and N. S. Leiws, *J. Appl. Phys.*, 2005, **97**, 114302.
13 T. C. Harman, P. J. Taylor, M. P. Walsh and B. E. LaForge, *Science*, 2002, **297**, 2229.
14 K. F. Hsu, S. Loo, F. Guo, W. Chen, J. S. Dyck, C. Uher, T. Hogan, E. K. Polychroniadis and M. G. Kanatzidis, *Science*, 2004, **303**, 818.
15 R. Venkatasubramanian, E. Siivoal, T. Colpitts and B. O'Quinn, *Nature*, 2001, **413**, 597.
16 Z. L. Wang, *Adv. Funct. Mater.*, 2008, **18**, 3553.
17 X. Wang, J. Song and Z. L. Wang, *J. Mater. Chem.*, 2007, **17**, 711.
18 C.-H. Cho, C. O. Aspetti, M. E. Turk, J. M. Kikkawa, S.-W. Nam and R. Agarwal, *Nat. Mater.*, 2011, **10**, 669.
19 J. A. Schuller, E. S. Barnard, W. Cai, Y. C. Jun, J. S. White and M. L. Brongersma, *Nat. Mater.*, 2010, **9**, 193.
20 E. C.-W. Ou, L. Hu, G. C. R. Raymond, O. K. Soo, J. Pan, Z. Zheng, Y. Park, D. Hecht, G. Irvin, P. Drzaic and G. Gruner, *ACS Nano*, 2009, **3**, 2258.
21 S. A. Mcdonald, G. Konstantatos, S. Zhang, P. W. Cyr, E. J. D. Klem, L. Levina and E. H. Sargent, *Nat. Mater.*, 2005, **4**, 138.
22 B. Lim, M. Jiang, P. H. C. Camargo, E. C. Cho, J. Tao, X. Lu, Y. Zhu and Y. Xia, *Science*, 2009, **324**, 1302.
23 D. R. Kauffman, D. C. Sorescu, D. P. Schofield, B. L. Allen, K. D. Jordan and A. Star, *Nano Lett.*, 2010, **10**, 958.
24 C. N. R. Rao, F. L. Deepark, G. Gundiah and A. Govindaraj, *Prog. Solid State Chem.*, 2003, **31**, 5.
25 X. Wang and Y. Li, *Inorg. Chem.*, 2006, **45**, 7522.
26 L. E. Bell, *Science*, 2008, **321**, 1457.
27 D. V. Talapin, J.-S. Lee, M. V. Kovalenko and E. V. Shevchenko, *Chem. Rev.*, 2010, **110**, 389.
28 H. Zhong, S. S. Lo, T. Mirkovic, Y. Li, Y. Ding, Y. Li and G. D. Scholes, *ACS Nano*, 2010, **4**, 5253.
29 M. He, F. Qiu and Z. Lin, *J. Phys. Chem. Lett.*, 2013, **4**, 1788.
30 G. Du, Z. Guo, S. Wang, R. Zeng, Z. Chen and H. Liu, *Chem. Commun.*, 2010, **46**, 1106.
31 H. Liu, D. Su, G. Wang and S. Z. Qiao, *J. Mater. Chem.*, 2012, **22**, 17437.
32 J.-W. Seo, J.-T. Jang, S.-W. Park, C. Kim, B. Park and J. Cheon, *Adv. Mater.*, 2008, **20**, 4269.
33 H. Hwang, H. Kim and J. Cho, *Nano Lett.*, 2011, **11**, 4826.
34 P. Chen, T.-Y. Xiao, H.-H. Li, J.-J. Yang, Z. Wang, H.-B. Yao and S.-H. Yu, *ACS Nano*, 2012, **6**, 712.
35 S. Liu, Z. Zhang, J. Bao, Y. Lan, W. Tu, M. Han and Z. Dai, *J. Phys. Chem. C*, 2013, **117**, 15164.
36 J. M. Luther, P. K. Jian, T. Ewers and A. P. Alivisatos, *Nat. Mater.*, 2011, **10**, 361.
37 S.-W. Hsu, K. On and A. R. Tao, *J. Am. Chem. Soc.*, 2011, **133**, 19072.
38 F. Xiu, L. He, Y. Wang, L. Cheng, L.-T. Chang, M. Lang, G. Huang, X. Kou, Y. Zhou, X. Jiang, Z. Chen, J. Zou, A. Shailos and K. L. Wang, *Nat. Nanotechnol.*, 2011, **6**, 216.
39 Z.-A. Ren and Z.-X. Zhao, *Adv. Mater.*, 2009, **21**, 4584.
40 C. Jiang, J.-S. Lee and D. V. Talapin, *J. Am. Chem. Soc.*, 2012, **134**, 5010.
41 M. G. Panthani, V. Akhavan, B. Goodfellow, J. P. Schmidtke, L. Dunn, A. Dodabalapur, P. F. Barbara and B. A. Korgel, *J. Am. Chem. Soc.*, 2008, **130**, 16770.
42 C. Steinhagen, M. G. Panthani, V. Akhavan, B. Goodfellow, B. Koo and B. A. Korgel, *J. Am. Chem. Soc.*, 2009, **131**, 12554.
43 Q. Guo, H. W. Hillhouse and R. Agrawal, *J. Am. Chem. Soc.*, 2009, **131**, 11672.
44 J. A. Venables, *Introduction to Surface and Thin Film Processes*, Cambridge University Press, Cambridge, 2000, p. 4.
45 B. Gates, B. Mayers, B. Cattle and Y. Xia, *Adv. Funct. Mater.*, 2002, **12**, 219.
46 B. Mayers and Y. Xia, *J. Mater. Chem.*, 2002, **12**, 1875.
47 S. Grimme, *J. Comput. Chem.*, 2006, **27**, 1787.

48 J. P. Perdew, K. Burke and M. Ernzerhof, *Phys. Rev. Lett.*, 1996, **77**, 3865.
49 P. E. Blöchl, *Phys. Rev. B: Condens. Matter Mater. Phys.*, 1994, **50**, 17953.
50 X. Gao, T. Gao and L. Zhang, *J. Mater. Chem.*, 2003, **13**, 6.
51 L. Ren, H. Zhang, P. Tan, Y. Chen, Z. Zhang, Y. Chang, J. Xu, F. Yang and D. Yu, *J. Phys. Chem. B*, 2004, **108**, 4627.
52 Z. Liu, S. Li, Y. Yang, Z. Hu, S. Peng, J. Liang and Y. Qian, *New J. Chem.*, 2003, **27**, 1748.
53 X. Cao, Y. Xie, S. Zhang and F. Li, *Adv. Mater.*, 2004, **16**, 649.
54 B. Gates, Y. Yin and Y. Xia, *J. Am. Chem. Soc.*, 2000, **122**, 12582.
55 B. Zhang, W. Dai, X. Ye, W. Hou and Y. Xie, *J. Phys. Chem. B*, 2005, **109**, 22830.
56 S. Xiong, B. Xi, W. Wang, C. Wang, L. Fei, H. Zhou and Y. Qian, *Cryst. Growth Des.*, 2006, **6**, 1711.
57 M. Mo, J. Zeng, X. Liu, W. Yu, S. Zhang and Y. Qian, *Adv. Mater.*, 2002, **14**, 1658.
58 Q. Lu, F. Gao and S. Komarneni, *Adv. Mater.*, 2004, **16**, 1629.
59 Z. Liu, Z. Hu, J. Liang, S. Li, Y. Yang, S. Peng and Y. Qian, *Langmuir*, 2004, **20**, 214.
60 Z. Liu, Z. Hu, Q. Xie, B. Yang, J. Wu and Y. Qian, *J. Mater. Chem.*, 2003, **13**, 159.
61 B. Xi, S. Xiong, H. Fan, X. Wang and Y. Qian, *Cryst. Growth Des.*, 2007, **7**, 1185.
62 B. Zhang, W. Hou, X. Ye, S. Fu and Y. Xie, *Adv. Funct. Mater.*, 2007, **17**, 486.
63 Z.-H. Lin, Z. Yang and H.-T. Chang, *Cryst. Growth Des.*, 2008, **8**, 353.
64 J.-W. Liu, J.-H. Zhu, C.-L. Zhang, H.-W. Liang and S.-H. Yu, *J. Am. Chem. Soc.*, 2010, **132**, 8945.
65 D. Qin, J. Zhou, C. Luo, Y. Liu, L. Han and Y. Cao, *Nanotechnology*, 2006, **17**, 674.
66 U. Jeong, Y. Xia and Y. Yin, *Chem. Phys. Lett.*, 2005, **416**, 246.
67 H.-S. Qian, S.-H. Yu, J.-Y. Gong, L.-B. Luo and L.-F. Fei, *Langmuir*, 2006, **22**, 3830.
68 G. D. Moon, Y. Min, S. Ko, S.-W. Kim, D.-H. Ko and U. Jeong, *ACS Nano*, 2010, **4**, 7283.
69 U. Mizutani, *Hume-Rothery Rules for Structurally Complex Alloy Phases*, CRC Press, London, 2008.
70 Y. Wang, J. Chen, P. Wang, L. Chen, Y.-B. Chen and L.-M. Wu, *J. Phys. Chem. C*, 2009, **113**, 16009.
71 R. Malakooti, L. Cademartiri, Y. Akcakir, S. Petrov, A. Migliori and G. A. Ozin, *Adv. Mater.*, 2006, **18**, 2189.
72 H. Zhang, Y. Ji, X. Ma, J. Xu and D. Yang, *Nanotechnology*, 2003, **14**, 974.
73 Y. Yu, R. H. Wang, Q. Chen and L.-M. Peng, *J. Phys. Chem. B*, 2006, **110**, 13415.
74 J. Ma, Y. Wang, Y. Wang, Q. Chen, J. Lian and W. Zheng, *J. Phys. Chem. C*, 2009, **113**, 13588.
75 A. Puzder, A. J. Williamson, N. Zaitseva, G. Galli, L. Manna and A. P. Alivisatos, *Nano Lett.*, 2004, **4**, 2361.
76 L. Manna, L. W. Wang, R. Cingolani and A. P. Alivisatos, *J. Phys. Chem. B*, 2005, **109**, 6183.
77 L. Qu, Z. A. Peng and X. Peng, *Nano Lett.*, 2001, **1**, 333.
78 A. Nag, A. Hazarika, K. V. Shanavas, S. M. Sharma, I. Dasgupta and D. D. Sarma, *J. Phys. Chem. Lett.*, 2011, **2**, 706.
79 Z. Liu, D. Xu, J. Liang, J. Shen, S. Zhang and Y. Qian, *J. Phys. Chem. B*, 2005, **109**, 10699.
80 E. Lifshitz, M. Bashouti, V. Kloper, A. Kigel, M. S. Eisen and S. Berger, *Nano Lett.*, 2003, **3**, 857.
81 P. Xue, R. Lu, D. Li, M. Jin, C. Tan, C. Bao, Z. Wang and Y. Zhao, *Langmuir*, 2004, **20**, 11234.
82 Q. Yan, H. Chen, W. Zhou, H. H. Hng, F. Y. C. Boey and J. Ma, *Chem. Mater.*, 2008, **20**, 6298.
83 W. Shi, J. Yu, H. Wang and H. Zhang, *J. Am. Chem. Soc.*, 2006, **128**, 16490.
84 R. Lv, C. Cao and H. Zhu, *Mater. Res. Bull.*, 2004, **39**, 1517.
85 R. Lv, C. Cao, H. Zhai, D. Wang, S. Liu and H. Zhu, *Solid State Commun.*, 2004, **130**, 241.
86 T. Sugimoto, *Adv. Colloid Interface Sci.*, 1987, **28**, 65.
87 J. W. Mullin, *Crystallization*, Butterworth-Heinemann, Stoneham, MA, 3rd edn, 1997.
88 Q. Zhang, S.-J. Liu and S.-H. Yu, *J. Mater. Chem.*, 2009, **19**, 191.
89 R. L. Penn and J. F. Banfield, *Am. Mineral.*, 1998, **83**, 1077.
90 R. L. Penn and J. F. Banfield, *Science*, 1998, **281**, 969.
91 J. F. Banfield, S. A. Welch, H. Zhang, T. T. Ebert and R. L. Penn, *Science*, 2000, **289**, 751.
92 Z. Tang, N. A. Kotov and M. Giersig, *Science*, 2002, **297**, 237.
93 F. Jiang, J. Liu, Y. Li, L. Fan, Y. Ding and Y. Li, *Adv. Funct. Mater.*, 2012, **22**, 2402.
94 N. Pradhan, H. Xu and X. Peng, *Nano Lett.*, 2006, **6**, 720.
95 W.-K. Koh, A. C. Bartnik, F. W. Wise and C. B. Murray, *J. Am. Chem. Soc.*, 2010, **132**, 3909.
96 K.-S. Cho, D. V. Talapin, W. Gaschler and C. B. Murray, *J. Am. Chem. Soc.*, 2005, **127**, 7140.
97 P. D. Cozzoli, L. Manna, M. L. Curri, S. Kudera, C. Giannini, M. Striccoli and A. Agostiano, *Chem. Mater.*, 2005, **17**, 1296.
98 G. Zhu, S. Zhang, Z. Xu, J. Ma and X. Shen, *J. Am. Chem. Soc.*, 2011, **133**, 15605.
99 B. B. Srivastava, S. Jana, D. D. Sarma and N. Pradhan, *J. Phys. Chem. Lett.*, 2010, **1**, 1932.
100 D. Moldovan, V. Yamakov, D. Wolf and S. R. Phillpot, *Phys. Rev. Lett.*, 2002, **89**, 206101.
101 E. R. Leite, T. R. Giraldi, F. M. Pontes, E. Longo, A. Beltran and J. Andres, *Appl. Phys. Lett.*, 2003, **83**, 1566.
102 Z. Zhuang, J. Zhang, F. Huang, Y. Wang and Z. Lin, *Phys. Chem. Chem. Phys.*, 2009, **11**, 8516.
103 H. Zheng, R. K. Smith, Y.-W. Jun, C. Kisielowski, U. Dahmen and A. P. Alivisatos, *Science*, 2009, **324**, 1309.
104 F. Huang, H. Zhang and J. F. Banfield, *Nano Lett.*, 2003, **3**, 373.
105 J. Zhang, Z. Lin, Y. Lan, G. Ren, D. Chen, F. Huang and M. Hong, *J. Am. Chem. Soc.*, 2006, **128**, 12981.
106 J. Zhang, Y. Wang, J. Zheng, F. Huang, D. Chen, Y. Lan, G. Ren, Z. Lin and C. Wang, *J. Phys. Chem. B*, 2007, **111**, 1449.
107 Z. Hu, G. Oskam, R. L. Penn, N. Pesika and P. C. Searson, *J. Phys. Chem. B*, 2003, **107**, 3124.

108 A. S. Barnard, H. Xu, X. Li, N. Pradhan and X. Peng, *Nanotechnology*, 2006, **17**, 5707.
109 D. V. Talapin, H. Yu, E. V. Shevchenko, A. Lobo and C. B. Murray, *J. Phys. Chem. C*, 2007, **111**, 14049.
110 S. A. Claridge, A. W. Castleman, S. N. Khanna, C. B. Murray, A. Sen and P. S. Weiss, *ACS Nano*, 2009, **3**, 244.
111 K. Liu, N. Zhao and E. Kumacheva, *Chem. Soc. Rev.*, 2011, **40**, 656.
112 M. Zanella, G. Bertoni, I. R. Franchini, R. Brescia, D. Baranov and L. Manna, *Chem. Commun.*, 2011, **47**, 203.
113 S. Ahmed and K. M. Ryan, *Chem. Commun.*, 2009, 6421.
114 K. M. Ryan, A. Mastroianni, K. A. Stancil, H. Liu and A. P. Alivisatos, *Nano Lett.*, 2006, **6**, 1479.
115 D. Kelly, A. Singh, C. A. Barrett, C. O'sSullivan, C. Coughlan, F. R. Laffir, C. O'Dwyer and K. M. Ryan, *Nanoscale*, 2011, **3**, 4580.
116 S. Gupta, Q. Zhang, T. Emrick and T. P. Russell, *Nano Lett.*, 2006, **6**, 2066.
117 D. D. Vaughn II, R. J. Patel, M. A. Hickner and R. E. Schaak, *J. Am. Chem. Soc.*, 2010, **132**, 15170.
118 J.-G. Kang, J.-G. Park and D.-W. Kim, *Electrochem. Commun.*, 2010, **12**, 307.
119 Y. Zhang, J. Lu, S. Shen, H. Xu and Q. Wang, *Chem. Commun.*, 2011, **47**, 5226.
120 D. D. Vaughn II, S.-I. In and R. E. Schaak, *ACS Nano*, 2011, **5**, 8852.
121 K. D. Oyler, X. Ke, I. T. Sines, P. Schiffer and R. E. Schaak, *Chem. Mater.*, 2009, **21**, 3655.
122 L. Chen, H. Zhan, X. Yang, Z. Sun, J. Zhang, D. Xu, C. Liang, M. Wu and J. Fang, *CrystEngComm*, 2010, **12**, 4386.
123 J. A. Wilson and A. D. Yoffe, *Adv. Phys.*, 1969, **18**, 193.
124 W. Jaegermann and H. Tributsch, *Prog. Surf. Sci.*, 1988, **29**, 1.
125 Y. Arnaud and M. Chevreton, *J. Solid State Chem.*, 1981, **39**, 230.
126 S. Jeong, D. Yoo, J.-T. Jang, M. Kim and J. Cheon, *J. Am. Chem. Soc.*, 2012, **134**, 18233.
127 V. V. Plashnitsa, F. Vietmeyer, N. Petchsang, P. Tongying, T. H. Kosel and M. Kuno, *J. Phys. Chem. Lett.*, 2012, **3**, 1554.
128 J.-T. Jang, S. Jeong, J.-W. Seo, M.-C. Kim, E. Sim, Y. Oh, S. Nam, B. Park and J. Cheon, *J. Am. Chem. Soc.*, 2011, **133**, 7636.
129 R. V. Coleman, B. Giambattista, P. K. Hansma, A. Johnson, W. W. McNairy and C. G. Slough, *Adv. Phys.*, 1988, **37**, 559.
130 R. H. Friend and D. Jerome, *J .Phys. C Solid State Phys.*, 1979, **12**, 1441.
131 L. Rapoport, Y. Bilik, Y. Feldman, M. Homyonfer, S. R. Cohen and R. Tenne, *Nature*, 1997, **387**, 791.
132 B. Radisavljevic, A. Radenovic, J. Brivio, V. Giacometti and A. Kis, *Nat. Nanotechnol.*, 2011, **6**, 147.
133 C. Lee, Q. Li, W. Kalb, X.-Z. Liu, H. Berger, R. W. Carpick and J. Hone, *Science*, 2010, **328**, 76.
134 J. Zhang, Z. Peng, A. Soni, Y. Zhao, Y. Xiong, B. Peng, J. Wang, M. S. Dresselhaus and Q. Xiong, *Nano Lett.*, 2011, **11**, 2407.
135 W. Lu, Y. Dong, Y. Chen, Z. L. Wang and J. Fang, *J. Am. Chem. Soc.*, 2005, **127**, 10112.
136 Y. Min, G. D. Moon, B. S. Kim, B. Lim, J.-S. Kim, C. Y. Kang and U. Jeong, *J. Am. Chem. Soc.*, 2012, **134**, 2872.
137 Y. Min, J. W. Roh, H. Yang, M. Park, S. I. Kim, S. Hwang, S. M. Lee, K. H. Lee and U. Jeong, *Adv. Mater.*, 2013, **25**, 1425.
138 W. Wang, B. Poudel, J. yang, D. Z. Wang and Z. F. Ren, *J. Am. Chem. Soc.*, 2005, **127**, 13792.
139 W. Shi, L. Zhou, S. Song, J. Yang and H. Zhang, *Adv. Mater.*, 2008, **20**, 1892.
140 F. Hulliger, *Structural chemistry of layer-type phases*, ed. B. F. A. Levy, D. Reidel publishing Company, Dordrecht, Holland, 1976, ch. 4, vol. 5, p. 91.
141 Y. Takemura, H. Suto, N. Honda, K. Kakuno and K. Saito, *J. Appl. Phys.*, 1997, **81**, 5177.
142 X. J. Wu, Z. Z. Zhang, J. Y. Zhang, Z. G. Ju, B. H. Li, B. S. Li, C. X. Shan, D. X. Zhao, B. Yao and D. Z. Shen, *Thin Solid Films*, 2009, **516**, 6116.
143 M. A. Malik, M. Afzaal and P. O'Brien, *Chem. Rev.*, 2010, **110**, 4417.
144 M. V. Kovalenko, M. Scheele and D. V. Talapin, *Science*, 2009, **324**, 1417.
145 W. Liu, J.-S. Lee and D. V. Talapin, *J. Am. Chem. Soc.*, 2013, **135**, 1349.
146 X. Peng, L. Manna, W. Yang, J. Wickham, E. Scher, A. Kadavanich and A. P. Alivisatos, *Nature*, 2000, **404**, 59.
147 J. S. Son, X.-D. Wen, J. Joo, J. Chae, S.-I. Baek, K. Park, J. H. Kim, K. An, J. H. Yu, S. G. Kwon, S.-H. Choi, Z. Wang, Y.-W. Kim, Y. Kuk, R. Hoffmann and T. Hyeon, *Angew. Chem., Int. Ed.*, 2009, **48**, 6861.
148 Z. Li and X. Peng, *J. Am. Chem. Soc.*, 2011, **133**, 6578.
149 J. Choi, N. Kang, H. Y. Yang, H. J. Kim and S. U. Son, *Chem. Mater.*, 2010, **22**, 3586.
150 S. Acharya, M. Dutta, S. Sarkar, D. Basak, S. Chakraborty and N. Pradhan, *Chem. Mater.*, 2012, **24**, 1779.
151 L. Jiang, Y.-J. Zhu and J.-B. Cui, *J. Solid State Chem.*, 2010, **183**, 2358.
152 B. Mahler, B. Nadal, C. Bouet, G. Patriarche and B. Dubertret, *J. Am. Chem. Soc.*, 2012, **134**, 18591.
153 S. Ithurria, G. Bousquet and B. Dubertret, *J. Am. Chem. Soc.*, 2011, **133**, 3070.
154 C. Xu, Y. Zeng, X. Rui, N. Xiao, J. Zhu, W. Zhang, J. Chen, W. Liu, H. Tan, H. H. Hng and Q. Yan, *ACS Nano*, 2012, **6**, 4713.
155 Z. Tang, Z. Zhang, Y. Wang, S. C. Glotzer and N. A. Kotov, *Science*, 2006, **314**, 274.
156 G. Zhang, W. Wang, X. Lu and X. Li, *Cryst. Growth Des.*, 2009, **9**, 145.
157 T. J. Zhu, X. Chen, X. Y. Meng, X. B. Zhao and J. He, *Cryst. Growth Des.*, 2010, **10**, 3727.
158 C. Schliehe, B. H. Juarez, M. Pelletier, S. Jander, D. Greshnykh, M. Nagel, A. Meyer, S. Foerster, A. Kornowski, C. Klinke and H. Weller, *Science*, 2010, **329**, 550.
159 Z. Wang, C. Schliehe, T. Wang, Y. Nagaoka, Y. C. Cao, W. A. Bassett, H. Wu, H. Fan and H. Weller, *J. Am. Chem. Soc.*, 2011, **133**, 14484.

160 J. S. Son, K. Park, S. G. Kwon, J. Yang, M. K. Choi, J. Kim, J. H. Yu, J. Joo and T. Hyeon, *Small*, 2012, **8**, 2394.
161 L. Li, Z. Chen, Y. Hu, X. Wang, T. Zhang, W. Chen and Q. Wang, *J. Am. Chem. Soc.*, 2013, **135**, 1213.
162 G. D. Moon, S. Ko, Y. Xia and U. Jeong, *ACS Nano*, 2010, **4**, 2307.
163 G. D. Moon, S. Ko, Y. Min, J. Zeng, Y. Xia and U. Jeong, *Nano Today*, 2011, **6**, 186.
164 H.-F. Shao, X.-F. Qian and Z.-K. Zhu, *J. Solid State Chem.*, 2005, **178**, 3522.
165 A. Cabot, R. K. Smith, Y. Yin, H. Zheng, B. M. Reinhard, H. Liu and A. P. Alivisatos, *ACS Nano*, 2008, **2**, 1452.
166 Y. Wang, L. Cai and Y. Xia, *Adv. Mater.*, 2005, **17**, 473.
167 H. Tan, S. Li and W. Y. Fan, *J. Phys. Chem. B*, 2006, **110**, 15812.
168 G. Zhang, Q. Yu, Z. Yao and X. Li, *Chem. Commun.*, 2009, 2317.
169 S. H. Kim and B. K. Park, *J. Appl. Phys.*, 2010, **108**, 102808.
170 J. Li, X. Tang, L. Song, Y. Zhu and Y. Qian, *J. Cryst. Growth*, 2009, **311**, 4467.
171 H. Fan, Y. Zhang, M. Zhang, X. Wang and Y. Qian, *Cryst. Growth Des.*, 2008, **8**, 2838.
172 B. Gates, B. Mayers, Y. Wu, Y. Sun, B. Cattle, P. Yang and Y. Xia, *Adv. Funct. Mater.*, 2002, **12**, 679.
173 A. K. Samal and T. Pradeep, *J. Phys. Chem. C*, 2009, **113**, 13539.
174 K. Wang, H.-W. Liang, W.-T. Yao and S.-H. Yu, *J. Mater. Chem.*, 2011, **21**, 15057.
175 H.-W. Liang, S. Liu, Q.-S. Wu and S.-H. Yu, *Inorg. Chem.*, 2009, **48**, 4927.
176 G. Tai, B. Zhou and W. Guo, *J. Phys. Chem. C*, 2008, **112**, 11314.
177 A. K. Samal and T. Pradeep, *J. Phys. Chem. C*, 2010, **114**, 5871.
178 A. Som and T. Pradeep, *Nanoscale*, 2012, **4**, 4537.
179 H. Zhu, J. Luo, H. Zhang, J. Liang, G. Rao, J. Li, G. Liu and Z. Du, *CrystEngComm*, 2012, **14**, 251.
180 U. Jeong, P. H. C. Camargo, Y. H. Lee and Y. Xia, *J. Mater. Chem.*, 2006, **16**, 3893.
181 J. M. Luther, H. Zheng, B. Sadtler and A. P. Alivisatos, *J. Am. Chem. Soc.*, 2009, **131**, 16851.
182 H. Li, M. Zanella, A. Genovese, M. Povia, A. Falqui, C. Giannini and L. Manna, *Nano Lett.*, 2011, **11**, 4964.
183 S. Jeong, J. H. Han, J.-T. Jang, J.-W. Seo, J.-G. Kim and J. Cheon, *J. Am. Chem. Soc.*, 2011, **133**, 14500.
184 V. R. Shinde, T. P. Gujar, T. Noda, D. Fujita, C. D. Lokhande and O.-S. Joo, *J. Phys. Chem. C*, 2009, **113**, 14179.
185 J. W. Kim, H.-S. Shim, S. Ko, U. Jeong, C.-L. Lee and W. B. Kim, *J. Mater. Chem.*, 2012, **22**, 20889.
186 I. T. Sines, D. D. Vaughn II, A. J. Biacchi, C. E. Kingsley, E. J. Popczun and R. E. Schaak, *Chem. Mater.*, 2012, **24**, 3088.
187 M. Mohl, A. Kumar, A. L. M. Reddy, A. Kuhovecz, Z. Konya, I. Kiricsi, R. Vajtai and P. M. Ajayan, *J. Phys. Chem. C*, 2010, **114**, 389.
188 J. H. Song, Y. Wu, B. Messer, H. Kind and P. Yang, *J. Am. Chem. Soc.*, 2001, **123**, 10397.
189 H.-W. Liang, S. Liu, J.-Y. Gong, S.-B. Wang, L. Wang and S.-H. Yu, *Adv. Mater.*, 2009, **21**, 1850.
190 H. Zhang, H. Wang, Y. Xu, S. Zhuo, Y. Yu and B. Zhang, *Angew. Chem., Int. Ed.*, 2012, **51**, 1459.
191 K. Chang and W. Chen, *Chem. Commun.*, 2011, **47**, 4252.
192 C. Altavilla, M. Sarno and P. Ciambelli, *Chem. Mater.*, 2011, **23**, 3879.
193 J. N. Coleman, M. Lotya, A. O'Neill, S. D. Bergin, P. J. King, U. Khan, K. Young, A. Gaucher, S. De, R. J. Smith, I. V. Shvets, S. K. Arora, G. Stanton, H.-Y. Kim, K. Lee, G. T. Kim, G. S. Duesbereg, T. Hallam, J. J. Boland, J. J. Wang, J. F. Donegan, J. C. Grunlan, G. Moriarty, A. Shmeliov, R. J. Nicholls, J. M. Perkins, E. M. Grieveson, K. Theuwissen, D. W. McComb, P. D. Nellist and V. Nicolosi, *Science*, 2011, **331**, 568.
194 G. Cunningham, M. Lotya, C. S. Cucinotta, S. Sanvito, S. D. Bergin, R. Menzel, M. S. P. Shaffer and J. N. Coleman, *ACS Nano*, 2012, **6**, 3468.
195 B. Luo, Y. Fang, B. Wang, J. Zhou, H. Song and L. Zhi, *Energy Environ. Sci.*, 2012, **5**, 5226.
196 W. Luo, Y. Xie, C. Wu and F. Zheng, *Nanotechnology*, 2008, **19**, 075602.
197 K. Chang and W. Chen, *ACS Nano*, 2011, **5**, 4720.
198 S. Ding, J. S. Chen and X. W. Lou, *Chem.–Eur. J.*, 2011, **17**, 13142.
199 S. K. Das, R. Mallavajula, N. Jayaprakash and L. A. Archer, *J. Mater. Chem.*, 2012, **22**, 12988.
200 Y. Idota, T. Kubota, A. Matsufuji, Y. Maekawa and T. Miyasaka, *Science*, 1997, **276**, 1395.
201 T. Zhai, L. Li, X. Wang, X. Fang, Y. Bando and D. Golberg, *Adv. Funct. Mater.*, 2010, **20**, 4233.
202 X. Fang, Y. Bando, M. Liao, U. K. Gautam, C. Zhi, B. Dierre, B. Liu, T. Zhai, T. Sekiguchi, Y. Koide and D. Golberg, *Adv. Mater.*, 2009, **21**, 2034.
203 T. Zhai, X. Fang, M. Liao, X. Xu, L. Li, B. Liu, Y. Koide, Y. Ma, J. Yao, Y. Bando and D. Golberg, *ACS Nano*, 2010, **4**, 1596.
204 J.-J. Wang, F.-F. Cao, L. Jiang, Y.-G. Guo, W.-P. Hu and L.-J. Wan, *J. Am. Chem. Soc.*, 2009, **131**, 15602.
205 J. S. Jie, W. J. Zhang, Y. Jiang, X. M. Meng, Y. Q. Li and S. T. Lee, *Nano Lett.*, 2006, **6**, 1887.
206 R. Zhou, H.-C. Chang, V. Protasenko, M. Kuno, A. K. Singh, D. Jena and H. Xing, *J. Appl. Phys.*, 2007, **101**, 073704.
207 X. Fang, S. Xiong, T. Zhai, Y. Bando, M. Liao, U. K. Gautam, Y. Koide, X. Zhang, Y. Qian and D. Golberg, *Adv. Mater.*, 2009, **21**, 5016.
208 T. Zhai, M. Ye, L. Li, X. Fang, M. Liao, Y. Li, Y. Koide, Y. Bando and D. Golberg, *Adv. Mater.*, 2010, **22**, 4530.
209 G. Konstantatos, L. Levina, J. Tang and E. H. Sargent, *Nano Lett.*, 2008, **8**, 4002.
210 G. Xiao, Q. Dong, Y. Wang, Y. Sui, J. Ning, Z. Liu, W. Tian, B. Liu, G. Zou and B. Zou, *RSC Adv.*, 2012, **2**, 234.
211 D. Wang, C. Hao, W. Zheng, Q. Peng, T. Wang, Z. Liao, D. Yu and Y. Li, *Adv. Mater.*, 2008, **20**, 2628.
212 J.-J. Wang, Y.-Q. Wang, F.-F. Cao, Y.-G. Guo and L.-J. Wan, *J. Am. Chem. Soc.*, 2010, **132**, 12218.

213 J.-J. Wang, J.-S. Hu, Y.-G. Guo and L.-J. Wan, *NPG Asia Mater.*, 2012, **4**, e2.
214 D.-J. Xue, J.-J. Wang, Y.-Q. Wang, S. Xin and Y.-G. Guo, *Adv. Mater.*, 2011, **23**, 3704.
215 X. Wang, W. Song, B. Liu, G. Chen, D. Chen, C. Zhou and G. Shen, *Adv. Funct. Mater.*, 2013, **23**, 1202.
216 B. C. Sales, *Science*, 2002, **295**, 1248.
217 M. S. Dresselhaus, G. Chen, M. Y. Tang, R. G. Yang, H. Lee, D. Z. Wang, Z. F. Ren, J. P. Fleurial and P. Gogna, *Adv. Mater.*, 2007, **19**, 1043.
218 G. J. Snyder and E. S. Toberer, *Nat. Mater.*, 2008, **7**, 105.
219 S. I. Kim, K. Ahn, D.-H. Yeon, S. Hwang, H.-S. Kim, S. M. Lee and K. H. Lee, *Appl. Phys. Express*, 2011, **4**, 091801.
220 D.-K. Ko, Y. Kang and C. B. Murray, *Nano Lett.*, 2011, **11**, 2841.
221 M. Scheele, N. Oeschler, I. Veremchuk, K.-G. Reinsberg, A.-M. Kreuziger, A. Kornowski, J. Broekaert, C. Klinke and H. Weller, *ACS Nano*, 2010, **4**, 4283.
222 A. Soni, Z. Yanyuan, Y. Ligen, M. K. K. Aik, M. S. Dresselhaus and Q. Xiong, *Nano Lett.*, 2012, **12**, 1203.
223 J. S. Son, M. K. Choi, M.-K. Han, K. Park, J.-Y. Kim, S. J. Lim, M. Oh, Y. Kuk, C. Park, S.-J. Kim and T. Hyeon, *Nano Lett.*, 2012, **12**, 640.
224 R. J. Mehta, Y. Zhang, C. Karthik, B. Singh, R. W. Siegel, T. Borca-Tasciuc and G. Ramanath, *Nat. Mater.*, 2012, **11**, 233.
225 G. Zhang, B. Kirk, L. A. Jauregui, H. Yang, X. Xu, Y. P. Chen and Y. Wu, *Nano Lett.*, 2012, **12**, 56.
226 W. Liang, O. Rabin, A. I. Hochbaum, M. Fardy, M. Zhang and P. Yang, *Nano Res.*, 2009, **2**, 394.
227 G. Zhang, H. Fang, H. Yang, L. A. Jauregui, Y. P. Chen and Y. Wu, *Nano Lett.*, 2012, **12**, 3627.
228 X. Z. Wu, *Sol. Energ.*, 2004, **77**, 803.
229 A. Romeo, M. Terheggen, D. Abou-Ras, D. L. Batzner, F.-J. Haug, M. Kalin, D. Rudmann and A. N. Tiwari, *Prog. Photovoltaics*, 2004, **12**, 93.
230 M. Kemell, M. Ritala and M. Leskela, *Crit. Rev. Solid State Mater. Sci.*, 2005, **30**, 1.
231 B. D. Weil, S. T. Connor and Y. Cui, *J. Am. Chem. Soc.*, 2010, **132**, 6642.
232 J. Puthussery, S. Seefeld, N. Berry, M. Gibbs and M. Law, *J. Am. Chem. Soc.*, 2011, **133**, 716.
233 Y. Yu, P. V. Kamat and M. Kuno, *Adv. Funct. Mater.*, 2010, **20**, 1464.
234 C. Steinhagen, V. A. Akhavan, B. W. Goodfellow, M. G. Panthani, J. T. Harris, V. C. Holmberg and B. A. Korgel, *ACS Appl. Mater. Interfaces*, 2011, **3**, 1781.
235 I. Gur, N. A. Fromer, M. L. Geier and A. P. Alivisatos, *Science*, 2005, **310**, 462.
236 Z. Feng, Q. Zhang, L. Lin, H. Guo, J. Zhou and Z. Lin, *Chem. Mater.*, 2010, **22**, 2705.
237 Q. Guo, G. M. Ford, R. Agrawal and H. W. Hillhouse, *Prog. Photovoltaics*, 2013, **21**, 64.
238 Q. Guo, G. M. Ford, H. W. Hillhouse and R. Agrawal, *Nano Lett.*, 2009, **9**, 3060.
239 S. Jeong, B.-S. Lee, S. Ahn, K. Yoon, Y.-H. Seo, Y. Choi and B.-H. Ryu, *Energy Environ. Sci.*, 2012, **5**, 7539.
240 A. J. Wooten, D. J. Werder, D. J. Williams, J. L. Casson and J. A. Hollingsworth, *J. Am. Chem. Soc.*, 2009, **131**, 16177.
241 W. Bi, M. Zhou, Z. Ma, H. Zhang, J. Yu and Y. Xie, *Chem. Commun.*, 2012, **48**, 9162.
242 J. Xu, Y.-B. Tang, X. Chen, C.-Y. Luan, W.-F. Zhang, J. A. Zapien, W.-J. Zhang, H.-L. Kwong, X.-M. Meng, S.-T. Lee and C.-S. Lee, *Adv. Funct. Mater.*, 2010, **20**, 4190.
243 A. Singh, C. Coughlan, F. Laffir and K. M. Ryan, *ACS Nano*, 2012, **6**, 6977.
244 A. Singh, H. Geaney, F. Laffir and K. M. Ryan, *J. Am. Chem. Soc.*, 2012, **134**, 2910.
245 Y. Min, G. D. Moon, J. Park, M. Park and U. Jeong, *Nanotechnology*, 2011, **22**, 465604.
246 T. Xu and Q. Qiao, *Energy Environ. Sci.*, 2011, **4**, 2700.
247 M. D. McGehee, *MRS Bull.*, 2009, **34**, 95.
248 X. Fan, M. Zhang, X. Wang, F. Yang and X. Meng, *J. Mater. Chem. A*, 2013, **1**, 8694.
249 W. U. Huynh, J. J. Dittmer and A. P. Alivisatos, *Science*, 2002, **295**, 2425.
250 Y. Wu and G. Zhang, *Nano Lett.*, 2010, **10**, 1628.
251 B. Sun, H. J. Snaith, A. S. Dhoot, S. Westenhoff and N. C. Greenham, *J. Appl. Phys.*, 2005, **97**, 014914.
252 P. Wang, A. Abrusci, H. M. P. Wong, M. Svensson, M. R. Andersson and N. C. Greenham, *Nano Lett.*, 2006, **6**, 1789.
253 S. Dayal, N. Kopidakis, D. C. Olson, D. S. Ginley and G. Rumbles, *Nano Lett.*, 2010, **10**, 239.
254 J. A. Chang, J. H. Rhee, S. H. Im, Y. H. Lee, H.-J. Kim, S. I. Seok, M. K. Nazeeruddin and M. Gratzel, *Nano Lett.*, 2010, **10**, 2609.
255 S.-H. Im, C.-S. Lim, J. A. Chang, Y. H. Lee, N. Maiti, H.-J. Kim, Md. K. Nazeeruddin, M. Gratzel and S. I. Seok, *Nano Lett.*, 2011, **11**, 4789.
256 E. Hutter and J. H. Fendler, *Adv. Mater.*, 2004, **16**, 1685.
257 J. Homola, *Anal. Bioanal. Chem.*, 2003, **377**, 528.
258 J. Homola, *Chem. Rev.*, 2008, **108**, 462.
259 B. P. Nelson, T. E. Grimsrud, M. R. Lies, R. M. Goodman and R. M. Corn, *Anal. Chem.*, 2001, **73**, 1.
260 M. L. Brongersma, J. W. Hartman and H. A. Atwater, *Phys. Rev. B: Condens. Matter Mater. Phys.*, 2000, **62**, 16356.
261 E. Ozbay, *Science*, 2006, **311**, 189.
262 S.-W. Hsu, W. Bryks and A. R. Tao, *Chem. Mater.*, 2012, **24**, 3765.
263 J. S. Niezgoda, M. A. Harrison, J. R. McBride and S. J. Rosenthal, *Chem. Mater.*, 2012, **24**, 3294.
264 Y. Zhao, H. Pan, Y. Lou, X. Qiu, J. Zhu and C. Burda, *J. Am. Chem. Soc.*, 2009, **131**, 4253.
265 I. Kriegel, C. Jiang, J. Rodriguez-Fernandez, R. D. Schaller, D. V. Talapin, E. da Como and J. Feldmann, *J. Am. Chem. Soc.*, 2012, **134**, 1583.
266 M.-H. Shao, K. Sasaki and R. R. Adzic, *J. Am. Chem. Soc.*, 2006, **128**, 3526.
267 J. K. Norskov, J. Rossmeisl, A. Logadottir, L. Lindqvist, J. R. Kitchin, T. Bligaard and H. Jonsson, *J. Phys. Chem. B*, 2004, **108**, 17886.
268 M. Winter and R. J. Brodd, *Chem. Rev.*, 2004, **104**, 4245.
269 M.-R. Gao, J. Jiang and S.-H. Yu, *Small*, 2012, **8**, 13.

270 M.-R. Gao, S. Liu, J. Jiang, C.-H. Cui, W.-T. Yao and S.-H. Yu, *J. Mater. Chem.*, 2010, **20**, 9355.
271 J. G. Checkelsky, Y. S. Hor, R. J. Cava and N. P. Ong, *Phys. Rev. Lett.*, 2011, **106**, 196801.
272 D. Kong, Y. Chen, J. J. Cha, Q. Zhang, J. G. Analytis, K. Lai, Z. Liu, S. S. Hong, K. J. Koski, S.-K. Mo, Z. Hussain, I. R. Fisher, Z.-X. Shen and Y. Cui, *Nat. Nanotechnol.*, 2011, **6**, 705.
273 L. Fu, C. L. Kane and E. J. Mele, *Phys. Rev. Lett.*, 2007, **98**, 106803.
274 I. Garate and M. Franz, *Phys. Rev. Lett.*, 2010, **104**, 146802.
275 L. Fu and C. L. Kane, *Phys. Rev. Lett.*, 2008, **100**, 096407.
276 H. Zhang, C.-X. Liu, X.-L. Qi, X. Dai, Z. Fang and S.-C. Zhang, *Nat. Phys.*, 2009, **5**, 438.
277 Y. Xia, D. Qian, D. Hsieh, L. Wray, A. Pal, H. Lin, A. Bansil, D. Grauer, Y. S. Hor, R. J. Cava and M. Z. Hasan, *Nat. Phys.*, 2009, **5**, 398.
278 Y. L. Chen, J. G. Analytis, J.-H. Chu, Z. K. Liu, S.-K. Mo, X. L. Qi, H. J. Zhang, D. H. Lu, X. Dai, Z. Fang, S. C. Zhang, I. R. Fisher, Z. Hussain and Z.-X. Shen, *Science*, 2009, **325**, 178.
279 D. Hsieh, Y. Xia, L. Wray, D. Qian, A. Pal, J. H. Dil, J. Osterwalder, F. Meier, G. Bihlmayer, C. L. Kane, Y. S. Hor, R. J. Cava and M. Z. Hasan, *Science*, 2009, **323**, 919.
280 M. Nath, S. Kar, A. K. Raychaudhuri and C. N. R. Rao, *Chem. Phys. Lett.*, 2003, **368**, 690.
281 C. W. Dunnill, H. K. Edwards, P. D. Brown and D. H. Gregory, *Angew. Chem., Int. Ed.*, 2006, **45**, 7060.
282 N. C. Gresty, Y. Takabayashi, A. Y. Ganin, M. T. McDonald, J. B. Claridge, D. Giap, Y. Mizuguchi, Y. Takano, T. Kagayama, Y. Ohishi, M. Takata, M. J. Ropsseinsky, S. Margadonna and K. Prassides, *J. Am. Chem. Soc.*, 2009, **131**, 16944.
283 Y. Mizuguchi, F. Tomioka, S. Tsuda, T. Yamaguchi and Y. Takano, *Appl. Phys. Lett.*, 2009, **94**, 012503.
284 F.-C. Hsu, J.-Y. Luo, K.-W. Yeh, T.-K. Chen, T.-W. Huang, P. M. Wu, Y.-C. Lee, Y.-L. Huang, Y.-Y. Chu, D.-C. Yan and M.-K. Wu, *Proc. Natl. Acad. Sci. U. S. A.*, 2008, **105**, 14262.
285 B. C. Sales, A. S. Sefat, M. A. McGuire, R. Y. Jin, D. Mandrus and Y. Mozharivskyj, *Phys. Rev. B: Condens. Matter Mater. Phys.*, 2009, **79**, 094521.
286 S. Medvedev, T. M. McQueen, I. Trojan, T. Palasyuk, M. I. Eremets, R. J. Cava, S. Naghavi, F. Casper, V. Ksenofontov, G. Wortmann and C. Felser, *Nat. Mater.*, 2009, **8**, 630.
287 Y. Mizuguchi, F. Tomioka, S. Tsuda, T. Yamaguchi and Y. Takano, *J. Phys. Soc. Jpn.*, 2009, **78**, 074712.
288 J. Guo, S. Jin, G. Wang, S. Wang, K. Zhu, T. Zhou, M. He and X. Chen, *Phys. Rev. B: Condens. Matter Mater. Phys.*, 2010, **82**, 180520(R).
289 L. Malavasi and S. Margadonna, *Chem. Soc. Rev.*, 2012, **41**, 3897.
290 Y. Zhang, L. P. Hu, T. J. Zhu, J. Xie and X. B. Zhao, *Cryst. Growth Des.*, 2013, **13**, 645.
291 P. Laurino, R. Kikkeri and P. H. Seeberger, *Nat. Protoc.*, 2011, **6**, 1209.
292 B.-H. Kwon, K. G. Lee, T. J. Park, H. Kim, T. J. Lee, S. J. Lee and D. Y. Jeon, *Small*, 2012, **8**, 3257.